Front. Earth Sci. 2023, 17(2): 437–454
https://doi.org/10.1007/s11707-022-0996-z

RESEARCH ARTICLE

Geological implications of elements of the Pleistocene mudstone with different organism compositions and enrichment environments in the Qaidam Basin, China

Jinqi QIAO[1,2], Qingyong LUO (✉)[1,2], Chen ZHANG[1,3], Zhenxue JIANG[1,3]

1 State Key Laboratory of Petroleum Resources and Prospecting, China University of Petroleum, Beijing 102249, China
2 Basin and Reservoir Research Center, China University of Petroleum, Beijing 102249, China
3 Unconventional Natural Gas Research Institute, China University of Petroleum, Beijing 102249, China

Abstract Trace elements and rare earth elements (REEs) of two kinds of organic facies samples representing marginal and more basin-center deposits from Pleistocene lacustrine mudstones in the central Qaidam Basin were studied to understand the provenance, palaeotectonic setting, hydrothermal activity, palaeoredox conditions and sedimentary rate. The results show that the lacustrine mudstones were mainly derived from felsic sources with little contribution from ancient crustal sediments and no ultramafic (ophiolitic) source. The mudstones were deposited in a continental island arc tectonic setting, which is consistent with the tectonic evolution of the Cenozoic basin. Both two organic facies samples were hydrothermal in origin based on the ternary diagram of Ni–Zn–Co and normalized REE patterns. However, this does not mean that the water column in paleolake was affected by hydrothermal fluids *in situ*. This signal might indicate hydrothermal origins from hot springs related to active faults around the basin rather than the deep hydrothermal fluids entering the sediments via deep faculties based on the comprehensive analyses of normalized REE patterns, negative Eu_{anom} (Eu anomaly), Y/Ho, Sm/Yb, and Eu/Sm. Redox proxies including U/Th, Ni/Co, and Mn_{anom} values, are more sensitive for the studied samples indicating that most of the organic facies A samples were deposited under an oxygen-depleted condition, while the organic facies B samples were deposited under oxygen-rich conditions. Redox proxies of Ce_{anom} values are unavailable for the organic facies B samples due to hypersaline environments, and V/Cr and V/(V + Ni) are invalid for the organic facies A samples, possibly because of their organism composition. The low La_n/Yb_n values indicate high sedimentation rates, which is consistent with the average sedimentation rates of approximately 0.43 to 1.1 km/Ma. However, the La_n/Yb_n is more likely affected by the provenance of the studied samples, so it should be used with caution.

Keywords elements, lacustrine mudstone, Pleistocene, Qigequan Formation, Qaidam Basin

1 Introduction

The chemical composition of sediments is greatly determined by multiple factors including initial provenance composition, the processes of weathering, erosion, transport distance, sedimentation, and finally burial diagenesis (Johnsson, 1993). Some researchers (e.g., Bhatia, 1983; Roser and Korsch, 1986) have argued that the relationships exist between major elements' geochemistry characteristics and provenance, or even between and the tectonic setting of deposition. However, some scholars have emphasized against that using major elements to interpret tectonic settings (Armstrong-Altrin and Verma, 2005; Ryan and Williams, 2007). Meanwhile, major elements are generally used to indicate palaeoclimatic conditions due to their great climatic influence (Sun et al., 2009; Lv et al., 2021; Qiao et al., 2022; Wu et al., 2022). In contrast, several trace elements and rare earth elements (REEs), are considered to be chemically rather immobile during diagenesis and thus are preserved well in sedimentary rocks and recorded the signature of the source materials (Floyd et al., 1990; McLennan et al., 1993; Li et al., 2021a; Lv et al., 2021). In addition, palaeotectonic settings of sedimentary basins based on trace elements and REEs are considered relatively reliable compared to using major elements (Armstrong-Altrin and Verma, 2005; Ryan and Williams, 2007; Shi et al., 2007; LaMaskin et al., 2008). Compared to coarse-grained

Received May 1, 2022; accepted June 23, 2022

E-mail: qingyong.luo@cup.edu.cn

sediments, which may show sorting effects, the geochemical characteristics of fine-grained sediments (i.e., mudstones and shales) are considered to be more representative of the average crustal composition and maintain the original geochemical signatures of provenance due to the homogeneity of grain size and impermeability after deposition (McCulloch and Wasserburg, 1978; Bhat and Ghosh, 2001). So, the trace elements and REEs in shale and mudstones are widely used to interpret the provenance of sediments, palaeotectonic setting, hydrothermal activity, sedimentary rate as well as palaeoredox condition (Wen et al., 2007; Li et al., 2021a; Lv et al., 2021; Ali et al., 2022).

The Qaidam Basin, located in the north-eastern Tibetan Plateau, developed the largest Quaternary commercial microbial gas reservoirs in the world (Hanson et al., 2001; Dang et al., 2008) (Fig. 1). Based on the sediment budget, Cenozoic tectonic uplift events (e.g., Ritts and Biffi, 2001; Zhuang et al., 2011b) and related denudation and unroofing might have resulted in significant changes in the mudstone for the sediments in the basin. Therefore, the interpretation of the provenance of these sediments can provide valuable information for understanding the composition of rocks in the orogenic belt on the margin of the north-eastern Tibetan Plateau. At present, there are relatively few detailed provenance studies on Pleistocene sediments, even though many studies have focused on rocks from the current mountains surrounding the Qaidam Basin (e.g., Song et al., 2005, 2009; Zhang et al., 2008; Mattinson et al., 2009; Menold et al., 2009; Zhang et al., 2009). The Cenozoic sediments in the north-eastern Qaidam Basin are regarded from the Qilian Mountains based on the isotopic chronology of clastic minerals and petrology of sandstone (Ritts and Biffi, 2001; Rieser et al., 2005, 2006a, 2006b). In addition, whole-rock geochemical data of Jurassic to Neogene sediments in the northern Qaidam Basin have been studied to reconstruct the provenance and chemical weathering history (Jian et al., 2013).

However, as a very important geological historical period for the uplift of the Tibetan Plateau, there are relatively few papers focused on the geological and geochemical information based on trace elements and REEs for Pleistocene sediments and none for the Pleistocene mudstone in the central Qaidam Basin so far. Accordingly, this study focuses on trace elements and REEs geochemical data and relevant interpretations for the two organic facies of Pleistocene mudstone representing marginal and more basin-center deposits in the central Qaidam Basin, and aims to 1) reconstruct the provenance of these sediments and reconstruct these microbial gas source rock chemical compositions; 2) analyze the tectonic setting and contribution of ancient crustal sediments; 3) evaluate the sedimentation rate and redox conditions of the aqueous medium; and 4) determine if there are hot fluid activities of these microbial gas source rocks in this area. This study is based on previous studies documenting the organic geochemical and petrographic assessment (Qiao et al., 2021) as well as climate and environment conditions (Qiao et al., 2022) from the same samples.

2 Geological setting

The Qaidam Basin spans an area of approximately 1.2×10^5 km^2 at an elevation of 2700–3500 m. This rhomb-shaped intermontane basin is formed by large-scale faults creating a high relief toward three mountain ranges (Fang et al., 2007) and as a result of the convergence system in the north-eastern Tibetan Plateau (Tapponnier et al., 2001). These mountains range from 4 to over 5 km in altitudes and are the Eastern Kunlun Mountains lying to the south, the Altyn Tagh Range to the north-west, and the Qilian Mountains to the east (Fig. 1(a)). The relatively low elevation of the basin compared to the mean elevation of the Tibetan Plateau (> 4000 m) led to an accumulation of 3000–16000 m of Mesozoic–Cenozoic sedimentary succession, mostly deposited in lacustrine environments (Jian et al., 2013) on the metamorphic and igneous basement (Pang et al., 2005). The Mesozoic tectonic settings were affected by the evolution of the Neo–Tethys, Mongol–Okhotsk Ocean, Meso–Tethys, and the collisions of related blocks (Gehrels et al., 2011).

The evolution of the basin experienced with three tectonic-sedimentary stages: piedmont fault depression stage during the Mesozoic period; unified depression stage during the Paleogene–Neogene periods; and cyclic folding in the midwest and subsiding depression in the east during the Quaternary period (Dang et al., 2008). The tectonic evolution of the Cenozoic basin is related to the India–Eurasia collision as well as the rise, thickening, shortening, and lateral extrusion of the Tibetan Plateau (Harrison et al., 1992; Tapponnier et al., 2001; Royden et al., 2008). Structurally, there are Mesozoic fault blocks in the north and two Cenozoic depressions in the south and west (Pang et al., 2005). During the deposition of the Jurassic strata, the depocenters of the basin were located in the northern area and were moving westward during the Paleogene–Neogene periods. The depocenters moved eastward during the Pleistocene because of the collision with the Indian Plate during the late Himalayan orogeny (the end of Neogene) (Pang et al., 2005). According to the sedimentary sequence and basement structure, the basin can be divided into four first-order structural units (Fig. 1(b)): the western and northern Qaidam Uplifts as well as the Sanhu and Yiliping Depressions (Bao et al., 2017). Eleven second-order structural units can be further divided, including Delingha Fault Sag, Yuka–Hongshan Fault Sag, Gasi Fault Sag, Sai–Kun Fault Sag, Mangya Sag, Sanhu Sag, North Kunlun Fault Terrace, Dafengshan

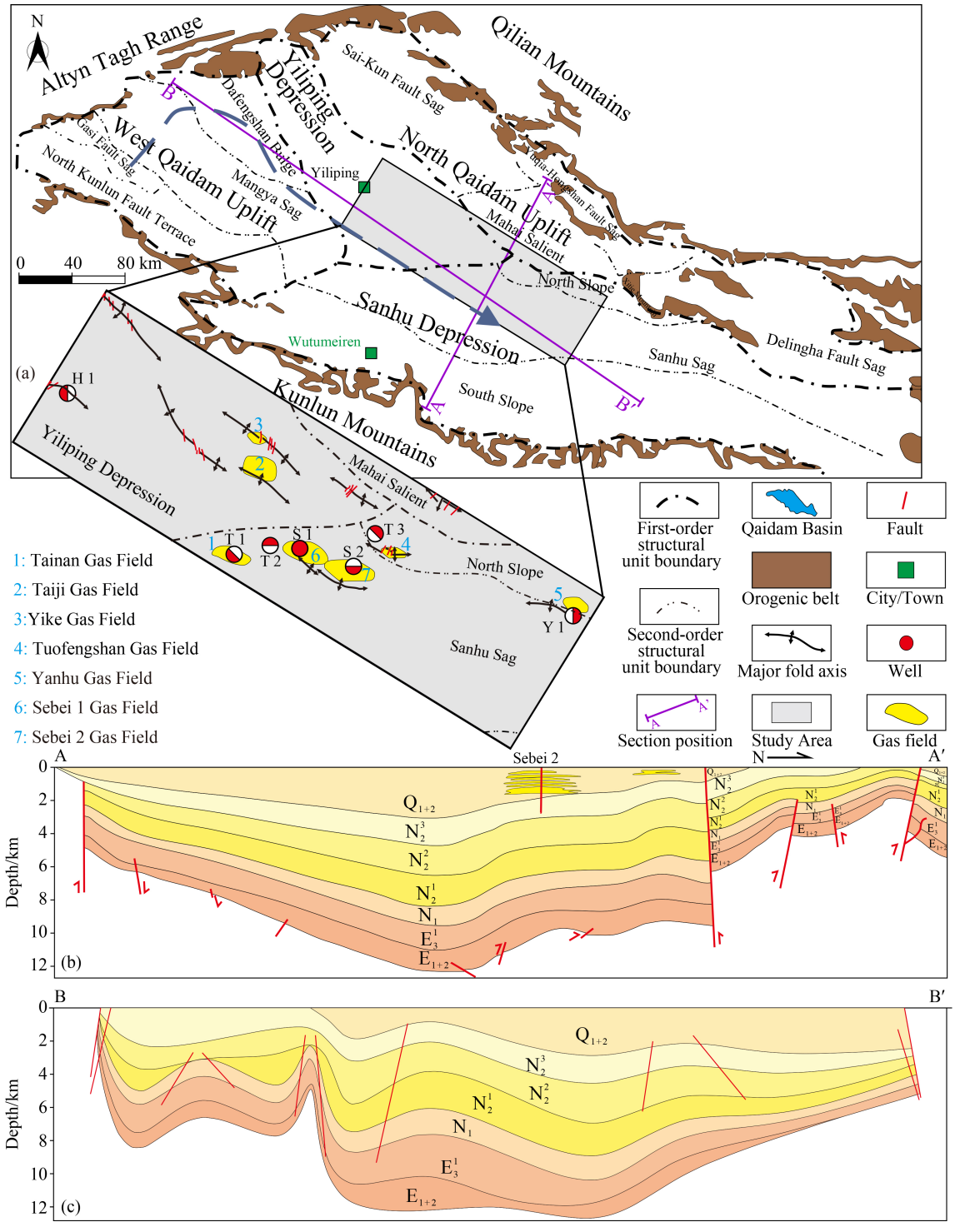

Fig. 1 (a) Geological setting and sample well locations, and (b and c) cross sections in SE–NE and NW–SE directions. The dashed line with an arrow illustrates the depocenter shift during the depositional history of the basin (Qiu et al., 2003).

Bulge, South Slope, North Slope, and Mahai Salient (Bao et al., 2017). In the early Pleistocene, a large number of terrestrial debris were deposited in fluvial–deltaic sediments. During the middle Pleistocene period, the lake basin reached its climax, with deposition dominated by deep-water fine-grained argillaceous sediments. In the late Pleistocene period, the central part of the basin was continuously uplifted under the influence of the neotectonic movement (Dang et al., 2008).

This study focuses on the central basin which developed the seven largest gas fields sourced from and trapped in near-shore, shallow, lacustrine sediments (Fig. 1(b); Shuai et al., 2013; Zhang et al., 2013a; Wang et al., 2015). A set of exceptionally thick Quaternary sediments,

i.e., the Pleistocene Qigequan Formation (Q_{1+2}), mostly varies between 1.5 and 2.5 km (avg. 1.7 km; greatest thickness approximately 3.4 km) and was deposited at rates of approximately 0.43 to 1.1 km/Ma (Figs. 1(c) and 1(d); Dang et al., 2008; Shuai et al., 2013; Zhang et al., 2013a; Qiao et al., 2021). This succession records detailed evidence of the geologic events including the collision between the Indian and Eurasian plates (Yin and Harrison, 2000; Royden et al., 2008), the formation and uplift of the Tibetan Plateau (Harrison et al., 1992; Tapponnier et al., 2001; Wang et al., 2008; Clark, 2011) and the aridification of Central Asia (Kutzbach et al., 1993; Molnar et al., 1993; Ramstein et al., 1997; An et al., 2001; Dupont-Nivet et al., 2007; Katz et al., 2008; Kent-Corson et al., 2009; Sun et al., 2010; Miao et al., 2011; Zhuang et al., 2011a). Based on seismic reflectance features, the Q_{1+2} Formation can be divided into 12 intervals (Zhang et al., 2013a; Fig. 2). The Maximum Flooding Surfaces (MFS) of a long–term sequence cycle corresponding to the middle Pleistocene (K_6–K_7) were deposited at the maximum expansion stage of the Q_{1+2} Formation (Fig. 2). The dominant lithology of the Q_{1+2} Formation is consistent with silty mudstones, mudstones, siltstones, and muddy limestones as well as some thin halite layers of 0.1 and 2.0 m thickness. Under the influence of the neotectonic movement during the late Pleistocene epoch, approximately 500 m of deposits were eroded along with the Sebei–Tainan gas fields during the Holocene, while slightly fewer sediments were eroded in the southern area of the Sanhu Depression (Zhang et al., 2013a).

3 Samples and methods

Twenty-eight fresh mudstone samples were sampled from seven drill holes for microbial gas exploration in the central Qaidam Basin (Fig. 1(b)) for whole-rock geochemical analyses. As observed by Zhang et al. (2014), two types are divided for these sediments in the study area according to total organic carbon (TOC) content, total sulfur (TS) content and lithologic characteristics.

The first type is defined as organic facies A, which has higher TOC and TS contents, coarser grain size, poor gradation, higher quartz and feldspar content, and lower

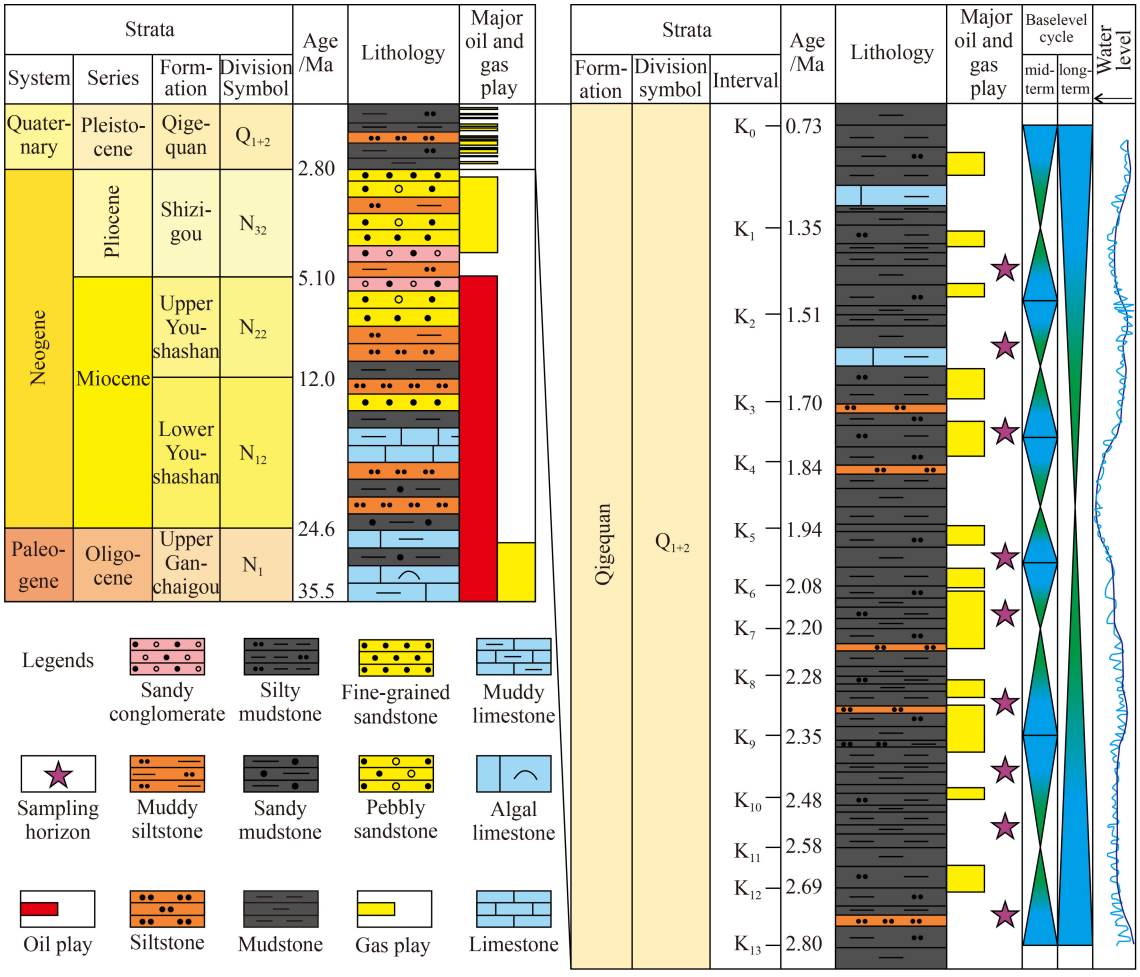

Fig. 2 Generalized Pleistocene stratigraphic column for the study area (modified after Jian et al., 2013 and Zhang et al., 2013a).

clay mineral content. The samples of organic phase A were deposited in lacustrine–marginal facies, e.g., shallow fluvial–lacustrine facies (Zhang et al. 2014). The second type is defined as organic phase B, which is characterized by low contents of TOC and TS, fine grain size, good gradation, and low contents of quartz and feldspar, but high contents of clay minerals with autogenic minerals account for about 10%–22%. Organic facies B samples were deposited in lacustrine facies (Zhang et al., 2014). The organic facies A samples examined in this study show both high TOC contents of 4.1 wt%–25.3 wt% and TS contents of 1.5 wt%–3.7 wt%, which formed in a shallow, freshwater fluvio–lacustrine environment with suboxic to anoxic redox conditions in the bottom water column. The environment is similar to inundated swamps developed during high water levels at the lake margins. Organic facies B samples are characterized by low TOC (0.5 wt%–1.1 wt%) and TS (0.14 wt%–1.0 wt%) contents developed under oxic conditions of bottom waters in more distal parts of the lake (Qiao et al., 2021). The most important organism composition for organic facies A is aquatic higher plants including macrophytes and submerged angiosperms, while the organic composition for organic facies B samples is mainly derived from saltwater algae. Cyanobacteria contributed to the organic matter (OM) in all samples, while another microbial contribution was more important for organic facies B than for organic facies A (Qiao et al., 2021). In addition, both organic facies A and B samples are immature (Qiao et al., 2021) and deposited under arid and cold palaeo-climate conditions (Qiao et al., 2022). All measurements concerning the above information were performed at the Institute of Geology and Geochemistry of Petroleum and Coal of RWTH Aachen University (Germany).

Before the measurement of trace elements and REEs, fresh core samples were pulverized to a fraction size of < 200 mesh using a tungsten carbide ball mill. The concentrations of trace elements and REEs were determined via an ELAN DRC–e inductively coupled plasma mass spectrometer (ICP–MS). Before the insertion into the ICP–MS, powders were digested with a mixed solvent of HF/HNO_3 in high–pressure Teflon bombs and then heated to 190°C for 48 h. Internal and international (BH–VO2, AGV–2, BCR–2 and GSP–1 from the United States Geological Survey (USGS)) standards were used for calibration and three duplicates were analyzed to investigate the accuracy of the measurements. The analytical accuracy and precision were < 10% and 5%, respectively. The measurements for the trace elements and REEs were performed at the Institute of Geochemistry, the Chinese Academy of Sciences.

4 Results and discussion

4.1 Provenance of sediments

The geochemical composition of sediments records the provenance information of the rocks from which they were derived. Some TTEs (e.g., Co and Sc) and HFSEs (e.g., Nb, Ta, Zr, Hf, and Th) as well as REEs, are preferred for use in the chemical discrimination of sediment provenance in sedimentary basins and to evaluate the relative contributions of felsic and basic sources because they are unlikely to disappear during the processes of transport and sedimentation (Taylor and McLennan, 1985; Bhatia and Crook, 1986; Cullers et al., 1987; Floyd and Leveridge, 1987; Nelson and DePaolo 1988; McLennan, 1989; McLennan and Taylor, 1991; McLennan et al., 1993; Cullers, 1995; Li et al., 2021a; Lv et al., 2021). The concentrations of elements used in this study are shown in Table1. The chondrite–normalized patterns of the studied mudstones are characterized by a sharp enrichment in LREEs (from La to Eu) and a fluctuation in HREEs (from Gd to Lu) with ΣLREE/ΣHREE ranging from 7.66 to 8.94 ppm (see Fig. 3 and Table 2).

In general, source types of the mudstones were analyzed using the plot of ΣREE − La/Yb. La/Yb values

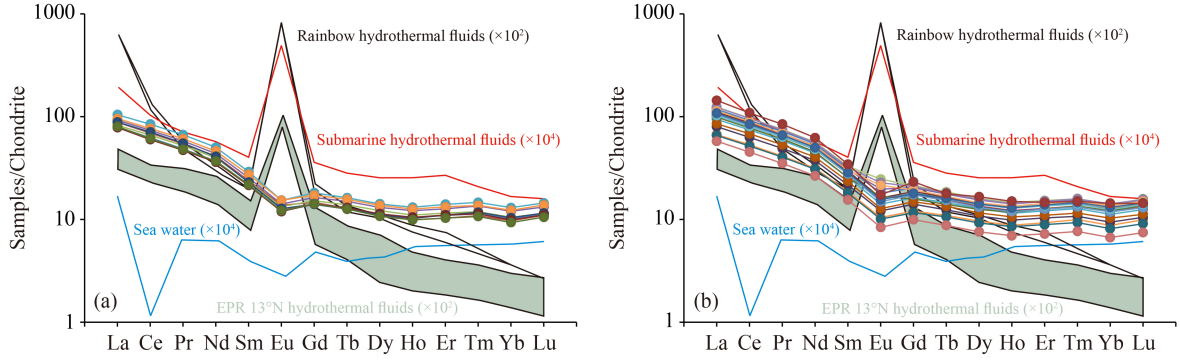

Fig. 3 Chondrite-normalized rare earth element patterns of (a) organic facies A and (b) B samples in comparison with the seawater (Piepgras and Jacobsen, 1992), 13°N hydrothermal fluids (Douville et al., 1999), Rainbow Vent hydrothermal fluids (Douville et al. 2002), and submarine hydrothermal fluids (Hongo et al., 2007) compositions.

Table 1 Elements concentrations (ppm) of the Pleistocene lacustrine mudstone from the Qaidam Basin, China

Well	Fm.	Sample ID	Depth/m	TOC [a]/%	Organic Facies	Fe [b]	Sc	Ti [c]	V	Cr	Mn [d]	Co	Ni	Y	Zr	La	Ce	Pr	Nd	Sm	Eu	Gd	Tb	Dy	Ho	Er	Tm	Yb	Lu	Hf	U [e]	Th [f]	MREE
S 1	K4	18-850	794.76	0.83	B	42987.00	14.23	4351.42	103.07	80.43	832.59	16.35	45.73	31.49	214.83	34.65	70.17	8.20	31.30	6.11	1.38	5.29	0.88	4.95	0.99	3.15	0.46	2.91	0.46	5.61	3.98	15.41	170.88
		18-853	801.46	12.86	A	27958.00	9.61	3686.73	72.61	64.59	442.50	11.32	47.16	24.48	171.48	25.60	53.60	6.27	23.87	4.66	0.93	3.96	0.69	3.91	0.77	2.43	0.36	2.20	0.34	4.41	14.89	10.75	129.59
		18-856	811.86	0.62	B	45850.00	18.26	4663.67	132.57	96.08	828.29	18.42	49.60	31.79	163.20	38.10	77.98	8.94	33.61	6.45	1.59	5.45	0.90	5.03	1.00	3.16	0.47	2.99	0.47	4.38	3.21	18.81	186.13
		18-857	820.47	0.78	B	37884.00	12.26	3266.87	87.62	68.14	876.52	14.85	41.66	26.81	180.73	31.99	65.31	7.59	28.75	5.51	1.10	4.61	0.76	4.23	0.84	2.66	0.40	2.49	0.39	4.65	2.77	14.06	156.63
	K9	18-858	1269.00	8.86	A	42532.00	12.65	4673.93	113.13	84.07	322.68	18.13	60.54	28.21	250.28	32.43	68.53	8.01	30.24	5.83	1.08	4.73	0.81	4.54	0.92	2.94	0.44	2.74	0.43	6.58	14.74	13.74	163.66
		18-860	1272.50	0.68	B	45787.00	15.71	4588.94	117.13	85.82	590.47	17.13	48.73	26.38	161.57	32.42	66.52	7.68	28.91	5.53	1.04	4.51	0.76	4.19	0.83	2.64	0.40	2.48	0.39	4.25	3.59	16.40	158.30
		18-861	1279.40	25.31	A	29036.00	9.32	3588.60	76.80	67.35	284.40	10.68	48.57	23.43	177.02	24.65	50.58	5.83	22.19	4.34	0.85	3.65	0.63	3.60	0.73	2.30	0.34	2.12	0.34	4.62	8.15	10.29	122.15
	K10	18-862	1377.50	16.73	A	49686.00	10.30	3669.33	186.74	95.33	350.79	13.92	59.53	22.69	393.74	27.37	56.21	6.55	24.82	4.79	0.96	3.82	0.64	3.48	0.70	2.17	0.33	2.04	0.33	6.68	19.26	12.30	134.20
		18-864	1380.50	6.49	A	51982.00	11.51	4782.43	113.92	90.85	272.69	20.90	88.30	23.05	279.05	27.52	57.43	6.62	24.59	4.60	0.89	3.67	0.63	3.54	0.72	2.32	0.35	2.18	0.35	5.86	13.40	13.23	135.42
T 1	K11	18-867	1697.30	4.08	A	25921.00	8.80	3204.03	85.71	59.29	742.82	9.74	38.72	23.31	168.26	24.88	49.64	5.76	22.24	4.36	0.85	3.69	0.63	3.44	0.69	2.17	0.32	1.96	0.32	3.95	9.93	9.40	120.95
		18-868	1697.50	4.15	A	27629.00	8.71	3106.79	86.25	57.12	1078.04	12.22	39.84	25.02	185.12	24.33	48.56	5.66	21.74	4.29	0.84	3.68	0.65	3.63	0.74	2.31	0.34	2.07	0.33	4.13	9.00	8.37	119.18
		18-869	1697.70	9.91	A	37779.00	12.28	4508.47	147.75	110.50	335.24	11.15	92.80	26.92	234.36	28.67	59.76	6.96	26.31	5.11	0.99	4.25	0.75	4.18	0.85	2.67	0.40	2.52	0.40	5.96	10.38	12.93	143.81
Y 1	K 4	18-872	124.69	0.64	B	46200.00	17.74	4722.24	132.68	95.03	687.46	17.56	48.27	32.45	158.39	38.51	78.44	9.00	33.92	6.58	1.72	5.55	0.93	5.12	1.02	3.20	0.48	2.94	0.47	4.23	4.79	19.56	187.86
		18-873	124.99	0.52	B	50743.00	17.93	4605.34	132.70	95.72	1063.60	19.54	49.42	29.28	161.33	35.20	72.59	8.23	31.06	6.02	1.50	5.04	0.84	4.65	0.94	3.01	0.45	2.85	0.45	4.30	3.18	18.26	172.85
S 2	K2	18-876	534.40	0.71	B	34510.00	16.39	3713.13	127.60	107.86	469.38	14.95	43.96	26.32	204.71	30.67	62.75	7.27	27.20	5.09	1.17	4.11	0.70	4.00	0.82	2.64	0.40	2.54	0.41	5.27	2.94	16.00	149.78
		18-878	543.80	8.19	A	34223.00	11.91	4421.07	86.88	75.60	416.02	12.52	59.58	27.50	229.62	29.67	62.24	7.30	27.81	5.49	1.07	4.48	0.78	4.38	0.88	2.79	0.41	2.58	0.41	5.96	15.19	12.56	150.30
	K3	18-879	555.10	1.11	B	48230.00	17.41	3591.42	124.20	95.69	1298.29	19.12	52.54	32.62	157.67	36.55	74.40	8.62	32.64	6.27	1.26	5.27	0.90	4.96	1.00	3.16	0.47	2.95	0.47	4.10	3.10	17.59	178.94
		18-880	566.10	1.10	B	39452.00	13.62	4248.90	98.97	74.39	924.22	14.53	40.89	27.97	154.36	32.66	66.07	7.62	28.86	5.58	1.10	4.65	0.78	4.31	0.86	2.68	0.40	2.48	0.40	4.03	3.48	14.78	158.45
	K7	18-892	1313.30	0.60	B	50617.00	17.79	4384.99	133.34	96.06	1023.23	18.93	51.07	29.13	147.93	33.47	68.04	7.88	29.40	5.61	1.10	4.70	0.80	4.50	0.91	2.90	0.44	2.73	0.43	3.97	3.93	17.40	162.90
	K10	18-894	1266.70	1.00	B	36218.00	11.15	3824.11	84.49	70.67	931.34	13.27	44.78	22.42	118.95	24.75	50.89	5.88	22.38	4.32	0.85	3.65	0.62	3.44	0.69	2.17	0.32	1.98	0.31	3.09	3.55	11.35	122.25
T 2	K6	18-895	1269.90	0.70	B	30807.00	10.85	3268.59	83.81	64.54	709.34	12.52	38.11	20.14	128.68	20.78	43.14	4.95	18.89	3.72	0.73	3.14	0.55	3.07	0.62	1.95	0.30	1.84	0.30	3.24	3.28	9.54	103.97
		18-897	235.10	0.79	B	28392.00	8.72	3200.11	66.26	50.60	1251.10	10.02	33.69	19.55	121.78	20.31	41.92	4.84	18.48	3.61	0.70	3.03	0.53	2.96	0.60	1.87	0.28	1.71	0.27	3.06	5.38	9.15	101.09
H 1	K4	18-898	255.90	0.70	B	31430.00	7.67	2548.00	58.50	44.29	496.20	8.76	25.52	15.73	86.73	17.87	36.67	4.21	15.91	3.10	0.59	2.58	0.44	2.42	0.48	1.52	0.23	1.40	0.22	2.23	6.50	8.20	87.65
		18-899	1082.70	0.66	B	38129.00	14.10	4421.42	103.13	76.57	955.94	15.36	43.26	29.26	157.90	31.76	64.87	7.57	28.89	5.61	1.09	4.72	0.79	4.45	0.90	2.83	0.42	2.62	0.42	4.13	5.28	14.28	156.96
	K13	18-900	982.20	0.69	B	32340.00	11.20	3963.05	84.76	63.56	1173.77	12.69	37.12	24.00	148.70	26.42	55.27	6.38	24.22	4.70	0.89	3.86	0.67	3.70	0.74	2.30	0.35	2.16	0.34	3.82	3.98	12.03	131.98
		18-901	985.80	0.82	B	39655.00	12.58	4295.16	95.51	69.99	726.64	14.60	42.22	26.18	150.32	29.18	60.16	7.01	26.49	5.14	0.99	4.23	0.73	4.10	0.80	2.54	0.38	2.35	0.37	3.86	3.77	12.84	144.47
T 3	K6	18-915	631.30	0.49	B	44709.00	17.34	3980.03	128.45	93.70	775.01	18.70	49.97	29.10	167.55	33.48	68.38	7.92	30.01	5.70	1.09	4.65	0.80	4.53	0.91	2.91	0.44	2.75	0.43	4.43	3.36	17.12	164.01
		18-916	646.11	0.77	B	39123.00	16.22	3393.65	116.23	93.91	853.70	19.06	52.74	29.16	189.87	34.45	71.03	8.21	30.92	5.91	1.13	4.85	0.82	4.55	0.91	2.86	0.42	2.63	0.42	4.91	4.06	16.31	169.12

Notes: [a] TOC, [b] Fe, [c] Ti, [d] Mn, [e] U, and [f] Th concentrations and more information about the samples have been reported by Qiao et al. (2021 and 2022).

and ΣREE values range from 11.32 to 13.41 (Table 2) and from 87.65 to 187.86 ppm (Table 1), respectively. In the ΣREE − La/Yb diagram, all sample data without clear differentiation values plot in the mixed area of sedimentary rock, granite, and basalt (Fig. 4(a)).

Generally, Sc is concentrated in mafic sources, and the variations in Th/Sc ratios indicate magmatic differentiation. In addition, Zr is mostly concentrated in zircons, which are stable to erosion and chemical weathering. Therefore, Zr easily accumulates during sedimentation. Therefore, the Zr/Sc ratio was used as an indicator for heavy mineral concentrations (Taylor and McLennan, 1985; McLennan, 1989). The first cycle sediments show a positive relationship between Th/Sc and Zr/Sc, which is controlled by the natural composition of the provenance rocks. In contrast, the variation in Th/Sc ratios is small, with a considerable variation in Zr/Sc ratios in more mature or cyclic sediments (McLennan et al., 1993). In the Th/Sc of 0.88–1.19 vs. Zr/Sc of 8.31–38.22 plot (Fig. 4(b); Table 2), the Th/Sc ratios in the mudstones show a highly fractionated and uniform source with composition clustering close to PAAS (Post–Archean Australian Shale; Taylor and McLennan, 1985) and UCC (upper continental crust). The Zr/Sc ratios in the mudstones show some variations, but no (or at least little) sediment recycling and sorting as represented by zircon enrichments (McLennan et al., 1993), so the studied samples can be used for provenance identification (Wu et al., 2022). The Eu_{anom} calculated via $Eu_N/(Sm_N \times Gd_N)^{1/2}$ (subscript N represents the chondrite–normalized value; the same for the following), and the ratio of ΣLREE/ΣHREE are affected by the chemical composition of the provenance. The felsic rocks show different degrees of negative Eu anomalies, while the basic rocks show little or no negative Eu anomalies (Cullers et al., 1987; Cullers, 1995). Moreover, Sc and Th are useful to assess the provenance area of sediments because Sc and Th are enriched in basic and felsic rocks, respectively, and there is no fractionation of these elements during the sedimentary cycle (Feng and Kerrich, 1990; McLennan et al., 1990). The negative Eu_{anom} (i.e., 0.61–0.93) and the ratio of Th/Sc ranging between 0.88 and 1.19 (Table 2) indicate that the majority of the samples are located in the field of the granitoids/felsic source (Fig. 5(a); McLennan et al., 1993; Cullers and Podkovyrov, 2002). Taylor and McLennan (1985) observed that the granitic rocks formed during Phanerozoic Eon have more K–feldspar rich granites, reflecting less Eu depletion and higher HREE depletion with a Gd_N/Yb_N ratio of < 2. The studied samples are similar to the post–Archean field with Gd_N/Yb_N = 1.31–1.53, indicating a felsic source as well. This is consistent with the high value of the ΣLREE/ΣHREE ratio (7.66–8.94; Table 2). The Hf vs. La/Th diagram (Floyd and Leveridge, 1987) is a useful indicator for whole–rock analysis to distinguish different arc sources. Mafic component–dominated arcs show low Hf values with high La/Th ratios of > 5, whereas felsic composition–dominated arcs are characterized by high Hf values and low La/Th ratios of < 5 (Fig. 5(b); Floyd and Leveridge 1987). This diagram shows that the two organic facies have similar characteristics. The uniformly low La/Th values (ranging between 1.92 and 2.91, averaging 2.20; Table 2) with Hf concentrations of 2.23–6.68 ppm (Table 1) for all analyzed samples indicate a predominant provenance from a felsic source with little contribution from ancient crustal sediments (Fig. 5(b)). In addition, La/Co and Cr/Th can be used to understand the provenance composition because La/Co in sediments from felsic sources (1.4–22.4) is higher than that from mafic sources (close to 0), whereas Cr/Th is lower from felsic sources (0.25–14.92) than that from mafic sources (> 22) (Cullers, 1994, 2000; Cullers and Podkovyrov, 2000). The La/Co (1.32–2.57) and Cr/Th (4.85–8.55) ratios of the studied samples listed in Table 2 are closer to the range of the felsic source, which is consistent with the above discussion.

Generally, it is believed that post–Archean shales have smaller concentrations of mafic elements, particularly Ni and Cr, than Archean crust (McLennan et al., 1983). Moreover, Cr of > 150 ppm, Ni of > 100 ppm and low Cr/Ni ratios ranging from 1.3 to 1.5 indicate some ultramafic rocks in the provenance (Garver et al., 1996). For the Pleistocene lacustrine microbial gas mudstone, the Ni and Cr concentrations are 25.52–92.80 ppm and 44.29–110.50 ppm (Table 1), respectively. On the Ni–Cr diagram (Taylor and McLennan, 1985) (Fig. 6), it is evident that mudstones plot in the post–Archean field, which also indicates their derivation from a felsic source (Condie, 1993). In addition, plots of Cr vs. Ni and Cr/V of 0.51–0.89 vs. Y/Ni of 0.26–0.69 (Table 2) (Hiscott, 1984) indicate no sample trends to ultramafic (ophiolitic) detritus in the provenance. It should be noted that the Cr/Ni ratios for all organic facies B samples are above 1.5, but only two of the nine organic facies A samples are above this value (Table 2). This might be due to the high palaeoproducitidy and redox conditions for the organic facies A samples.

Briefly, the provenance of sediments is a felsic source with little/no contribution from ancient crustal sediments or ultramafic (ophiolitic) sources. The same results were derived from the Cenozoic sediments in the northern Qaidam Basin based on elements (Jian et al., 2013) and Sr-Nd isotopes of gypsum in the western Qaidam Basin (Li et al., 2022). It should be noted that there is no significant difference between the two groups of samples in judging the provenance of sediments, indicating that the above–related proxies are not affected by the origin of OM and depositional environment.

4.2 Palaeotectonic setting

Tectonic setting discrimination diagrams based on major

Table 2 Calculated elemental ratios/normalized distribution of the Pleistocene lacustrine mudstones from the Qaidam Basin, China

Well	Fm.	Sample ID	Depth/m	TOC/%	Organic Facies	ΣLREE/ΣHREE	Eu_{anom} [a]	La/Yb	Th/Sc	Pr_{anom} [b]	Ce_{anom} [c]	Zr/Sc	La/Th	Y/Ni	Cr/V	Ti/Zr	La/Sc	La/Co	Cr/Th	Cr/Ni	Mn_{anom} [d]	La_n/Yb_n	U/Th	V/Cr	Ni/Co	V/(V+Ni)	Gd_N/Yb_N	Y/Ho	Eu/Sm	Sm/Yb	Normalized distribution of La-Th-Sc/%			Normalized distribution of Zr/10-Th-Sc/%			Normalized distribution of Ni-Zr-Co/%		
																															La	Th	Sc	Zr/10	Th	Sc	Ni	Zr	Co
S 1	K4	18-850	794.76	0.83	B	7.96	0.69	11.93	1.08	0.99	0.97	15.10	2.25	0.69	0.78	20.26	2.44	2.12	5.22	1.76	0.17	0.81	0.26	1.28	2.80	0.69	1.47	31.83	0.23	2.10	54	24	22	42	30	28	29	60	10
		18-853	801.46	12.86	A	7.84	0.73	11.63	1.12	0.99	0.97	17.84	2.38	0.52	0.89	21.50	2.66	2.26	6.01	1.37	0.09	0.79	1.38	1.12	4.17	0.61	1.45	31.71	0.20	2.12	56	23	21	46	29	26	40	51	10
		18-856	811.86	0.62	B	8.56	0.71	12.76	1.03	0.99	0.99	8.94	2.02	0.64	0.72	28.58	2.09	2.07	5.11	1.94	0.14	0.86	0.17	1.38	2.69	0.73	1.47	31.86	0.25	2.16	51	25	24	31	35	34	26	65	10
		18-857	820.47	0.78	B	8.56	0.69	12.87	1.15	0.99	0.97	14.74	2.28	0.64	0.78	18.08	2.61	2.15	4.85	1.64	0.25	0.87	0.20	1.29	2.80	0.68	1.50	31.75	0.20	2.22	55	24	21	41	32	28	29	61	10
	K9	18-858	1269.00	8.86	A	8.33	0.67	11.85	1.09	0.99	0.97	19.78	2.36	0.47	0.74	18.67	2.56	1.79	6.12	1.39	-0.23	0.80	1.07	1.35	3.34	0.65	1.40	30.68	0.18	2.13	55	23	22	49	27	25	39	49	12
		18-860	1272.50	0.68	B	8.77	0.70	13.05	1.04	0.99	0.98	10.28	1.98	0.54	0.73	28.40	2.06	1.89	5.23	1.76	0.00	0.88	0.22	1.36	2.84	0.71	1.47	31.67	0.19	2.23	50	25	24	33	34	33	28	62	10
		18-861	1279.40	25.31	A	7.90	0.71	11.61	1.10	0.98	0.98	18.98	2.40	0.48	0.88	20.27	2.64	2.31	6.55	1.39	-0.12	0.78	0.79	1.14	4.55	0.61	1.39	32.11	0.11	2.04	56	23	21	47	28	25	41	50	9
	K10	18-862	1377.50	16.73	A	8.94	0.69	13.41	1.19	0.99	0.97	38.22	2.22	0.38	0.51	9.32	2.66	1.97	7.75	1.60	-0.27	0.91	1.57	1.96	4.28	0.76	1.51	32.59	0.20	2.35	55	25	21	64	20	17	37	55	9
		18-864	1380.50	6.49	A	8.84	0.69	12.61	1.15	1.00	0.99	24.25	2.08	0.26	0.80	17.14	2.39	1.32	6.87	1.03	-0.39	0.85	1.01	1.25	4.23	0.56	1.36	32.04	0.19	2.11	53	25	22	53	25	22	48	41	11
T 1	K11	18-867	1697.30	4.08	A	8.15	0.72	12.68	1.07	0.98	0.97	19.11	2.65	0.60	0.69	19.04	2.83	2.55	6.31	1.53	0.34	0.86	1.06	1.45	3.97	0.69	1.52	33.61	0.20	2.22	58	22	20	48	27	25	38	52	10
		18-868	1697.50	4.15	A	7.66	0.71	11.73	0.96	0.99	0.96	21.25	2.91	0.63	0.66	16.78	2.79	1.99	6.83	1.43	0.48	0.79	1.08	1.51	3.26	0.68	1.43	33.99	0.19	2.07	59	20	21	52	24	24	38	51	12
		18-869	1697.70	9.91	A	7.98	0.70	11.38	1.05	0.99	0.97	19.08	2.22	0.29	0.75	19.24	2.33	2.57	8.55	1.19	-0.17	0.77	0.80	1.34	8.32	0.61	1.36	31.61	0.19	2.03	53	24	23	48	27	25	50	44	6
Y 1	K 4	18-872	124.69	0.64	B	8.54	0.79	13.11	1.10	0.99	0.99	8.93	1.97	0.67	0.72	29.81	2.17	2.19	4.86	1.97	0.06	0.89	0.24	1.40	2.75	0.73	1.53	31.79	0.26	2.24	51	26	23	30	37	33	25	65	9
		18-873	124.99	0.52	B	8.48	0.69	12.37	1.02	0.98	1.00	9.00	1.93	0.59	0.72	28.55	1.96	1.80	5.24	1.94	0.21	0.84	0.17	1.39	2.53	0.73	1.43	31.08	0.25	2.12	49	26	25	31	35	34	26	64	10
S 2	K2	18-876	534.40	0.71	B	8.58	0.70	12.07	0.98	0.99	0.98	12.49	1.92	0.60	0.85	18.14	1.87	2.05	6.74	2.45	0.02	0.82	0.18	1.18	2.94	0.74	1.31	32.07	0.23	2.00	49	25	26	39	30	31	27	64	9
		18-878	543.80	8.19	A	7.99	0.71	11.51	1.05	0.99	0.96	19.28	2.36	0.46	0.87	19.25	2.49	2.37	6.02	1.27	-0.03	0.78	1.21	1.15	4.76	0.59	1.40	31.15	0.20	2.13	55	23	22	48	26	25	42	50	9
	K3	18-879	555.10	1.11	B	8.32	0.69	12.37	1.01	0.99	0.98	9.06	2.08	0.62	0.77	22.78	2.10	1.91	5.44	1.82	0.32	0.84	0.18	1.30	2.75	0.70	1.44	32.55	0.20	2.12	51	25	24	31	35	34	28	62	10
		18-880	566.10	1.10	B	8.57	0.84	13.16	1.09	0.99	0.98	11.34	2.21	0.68	0.75	27.53	2.40	2.25	5.03	1.82	0.26	0.89	0.24	1.33	2.81	0.71	1.51	32.69	0.20	2.25	53	24	22	35	34	31	28	62	10
	K7	18-892	1313.30	0.60	B	8.36	0.70	12.26	0.98	1.00	0.99	8.31	1.92	0.57	0.72	29.64	1.88	1.77	5.52	1.88	0.19	0.83	0.19	1.39	2.70	0.72	1.39	31.88	0.20	2.05	49	25	26	30	35	36	27	63	10
	K10	18-894	1266.70	1.00	B	8.27	0.69	12.51	1.02	0.98	0.98	10.67	2.18	0.50	0.84	32.15	2.22	1.86	6.23	1.58	0.30	0.85	0.47	1.20	3.37	0.65	1.49	32.50	0.20	2.18	52	24	24	35	33	32	33	57	10
T 2	K6	18-895	1269.90	0.70	B	7.84	0.68	11.32	0.88	0.98	0.98	11.86	2.18	0.53	0.77	25.40	1.92	1.66	6.77	1.69	0.25	0.76	0.68	1.30	3.04	0.69	1.38	32.70	0.20	2.03	50	23	26	39	29	33	31	58	10
		18-897	235.10	0.79	B	8.00	0.68	11.89	1.05	0.98	0.98	13.97	2.22	0.58	0.76	26.28	2.33	2.03	5.53	1.50	0.53	0.80	0.58	1.31	3.36	0.66	1.43	32.78	0.19	2.12	53	24	23	41	30	29	33	57	10
H 1	K4	18-898	255.90	0.70	B	8.43	0.68	12.77	1.07	0.99	0.99	11.31	2.18	0.62	0.76	29.38	2.33	2.04	5.40	1.74	0.08	0.86	0.48	1.32	2.91	0.70	1.49	32.44	0.19	2.21	53	24	23	35	33	31	29	61	10
		18-899	1082.70	0.66	B	8.14	0.93	12.13	1.01	0.99	0.97	11.20	2.22	0.68	0.74	28.00	2.25	2.07	5.36	1.77	0.29	0.82	0.25	1.35	2.82	0.70	1.46	32.56	0.19	2.14	53	24	23	36	32	32	29	61	10
	K13	18-900	982.20	0.69	B	8.35	0.87	12.25	1.07	0.99	0.98	13.28	2.20	0.65	0.75	26.65	2.36	2.08	5.28	1.71	0.45	0.83	0.33	1.33	2.93	0.70	1.45	32.44	0.19	2.18	53	24	23	39	32	29	32	57	11
		18-901	985.80	0.82	B	8.31	0.69	12.40	1.02	0.99	0.97	11.95	2.27	0.62	0.73	28.57	2.32	2.00	5.45	1.66	0.15	0.84	0.29	1.36	2.89	0.69	1.45	32.53	0.19	2.18	53	24	23	37	32	31	24	68	8
T 3	K6	18-915	631.30	0.49	B	8.41	0.88	12.15	0.99	0.99	0.98	9.66	1.96	0.58	0.73	23.75	1.93	1.79	5.47	1.88	0.12	0.82	0.20	1.37	2.67	0.72	1.36	32.07	0.19	2.07	49	25	26	33	33	34	27	63	10
		18-916	646.11	0.77	B	8.68	0.69	13.09	1.01	0.99	0.98	11.71	2.11	0.55	0.81	17.87	2.12	1.81	5.76	1.78	0.22	0.88	0.25	1.24	2.77	0.69	1.49	32.04	0.19	2.24	51	24	24	37	32	31	29	60	11

Notes: [a] $Eu_{anom} = Eu_N/(Sm_N \times Gd_N)^{1/2}$; [b] $Pr_{anom} = Pr_n/(0.5 \times (La_n + Nd_n))$; [c] $Ce_{anom} = Ce_n/(0.5 \times (La_n + Pr_n))$; [d] $Mn_{anom} = \log (Mn_n/Fe_n)$. Subscript N and n represent the chondrite-and PAAS-normalized values, respectively.

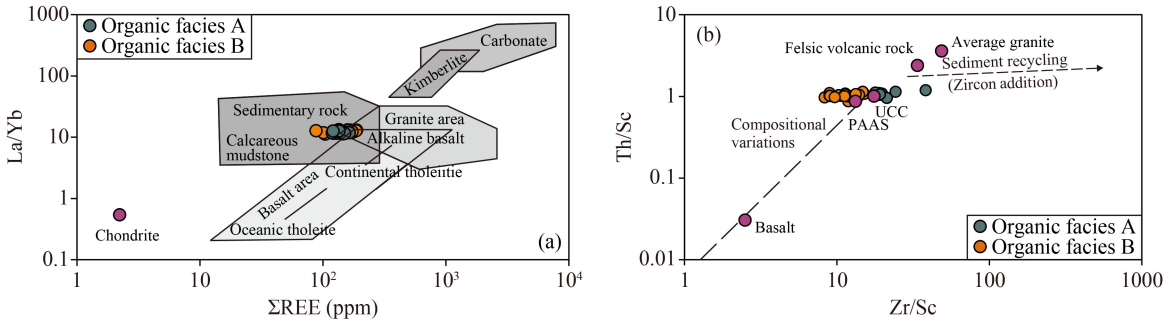

Fig. 4 (a) La/Yb vs. ΣREE illustrating source rocks of samples (after Allègre and Minster, 1978) and (b) Th/Sc vs. Zr/Sc illustrating weathering and sediment recycling (after McLennan et al., 1993).

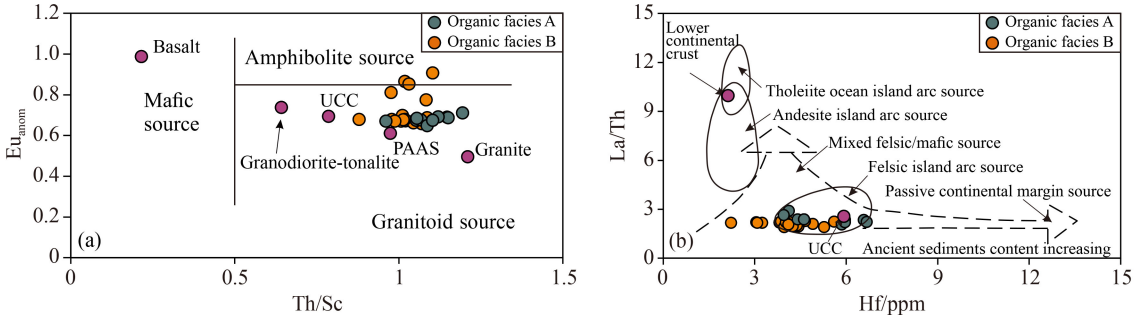

Fig. 5 (a) Th/Sc vs. Eu_{anom} (after McLennan et al., 1993; Cullers and Podkovyrov, 2002) and (b) La/Th vs. Hf (after Floyd and Leveridge, 1987) for sediments discrimination. $Eu_{anom} = Eu_N/(Sm_N \times Gd_N)^{1/2}$.

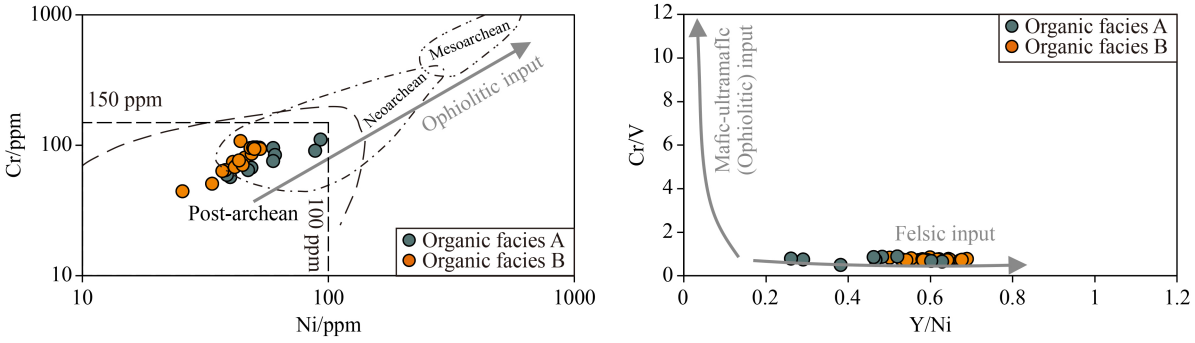

Fig. 6 Distributions of (a) Ni vs. Cr (fields are after Condie, 1993) and (b) Cr/V vs. Y/Ni (after Hiscott, 1984) for the studied samples.

elements are proposed by Bhatia (1983) and Roser and Korsch (1986). However, these discrimination plots have received considerable criticism (Armstrong-Altrin and Verma, 2005; Ryan and Williams, 2007). In addition to major elements, geochemical indices based on trace elements and REEs have been proposed to determine the palaeotectonic setting of sedimentary basins (Bhatia, 1983; Bhatia and Crook, 1986; Roser and Korsch, 1986), which are considered relatively reliable (LaMaskin et al., 2008). In these diagrams, continental margins and oceanic basins were divided into four tectonic types by Bhatia (1983), e.g., passive continental margins, oceanic island arcs, active continental margins, and continental island arcs.

The La–Th–Sc ternary diagram (Fig. 7(a)) shows that all samples with higher La but lower Sc concentrations are distributed in the continental island arc domain. Similar to what Fig. 7(a) shows, the Th–Sc–Zr/10 diagram (Fig. 7(b)) indicates that the mudstone samples plot in continental arc fields. Moreover, Figs. 7(a) and 7(b) indicate a predominance of felsic source composition because Sc is enriched in mafic igneous rocks (Taylor and McLennan, 1985; McLennan et al., 1993). Similar to the above results, most of the samples are clustered in the field of continental island arcs in the Ti/Zr vs. La/Sc plot after Bhatia and Crook (1986) (Fig. 8), where Ti/Zr and La/Sc ratios are 9.32–32.15 and 1.87–2.83, respectively (Table 2).

Therefore, we infer from the geochemistry of the mudstones that a stable and intracratonic tectonic setting existed during the deposition of the Q_{1+2} Formation sediments, which is consistent with the tectonic evolution of the Cenozoic basin related to the India–Eurasia collision (Harrison et al., 1992; Tapponnier et al., 2001;

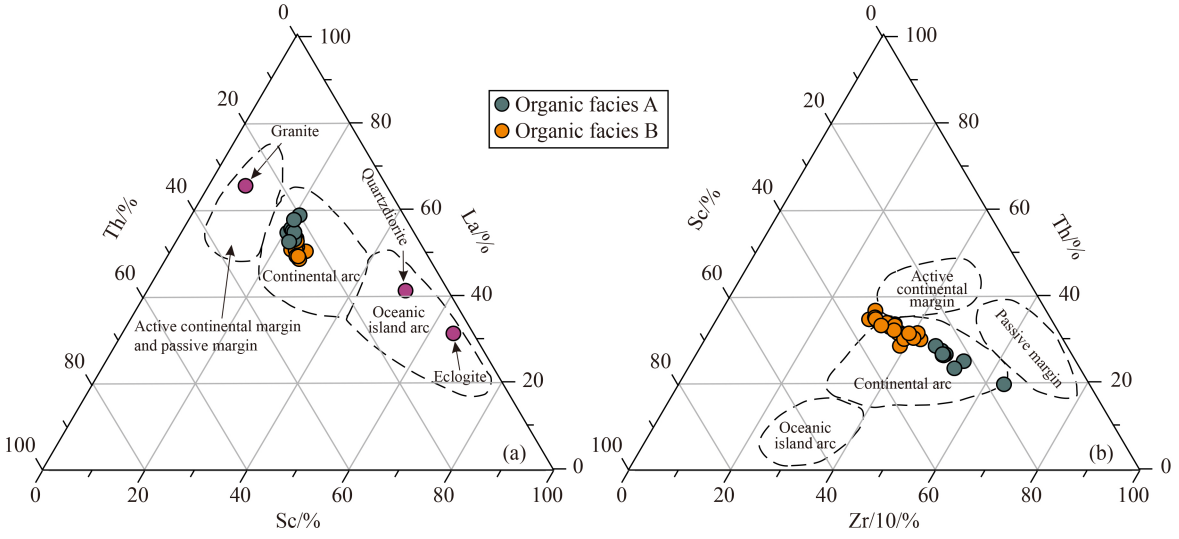

Fig. 7 (a) La-Th-Sc and (b) Th-Sc-Zr/10 (both after Bhatia and Crook, 1986) tectonic discrimination diagrams for the studied samples.

Royden et al., 2008). The two organic facies samples show different distributions in judging palaeotectonic settings, although all of them show consistency.

4.3 Hydrothermal activity

Generally, Co is mainly of hydrogenous origin, while Zn, Cu, and Ni are mainly of hydrothermal origin (Crerar, 1980; Choi and Hariya, 1992). Both organic facies A and B samples were hydrothermal in origin, as illustrated by the ternary diagram of Ni–Zn–Co (Fig. 9). Local hydrothermal activity is also indicated by the oilfield waters (Li et al., 2021b) and salt lakes (Yu et al., 2013) with significant Li–enrichment in the Qaidam Basin. In addition, the normalized REE patterns of both organic facies A and B samples are completely different from the seawater (Piepgras and Jacobsen, 1992), but similar to kinds of hydrothermal fluid compositions (Fig. 3) (Douville et al., 1999; Douville et al., 2002; Hongo et al., 2007). However, there is a clear difference between the studied samples and hydrothermal fluids, i.e., En. The lower En concentrations which are smaller than two adjacent

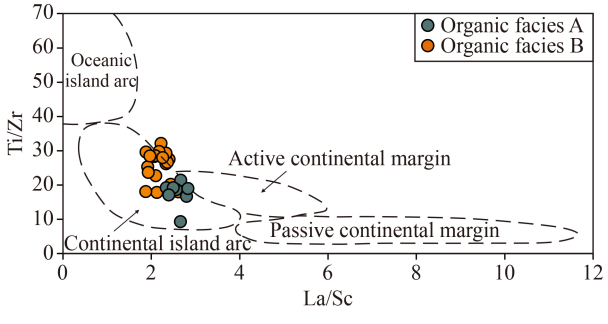

Fig. 8 Ti/Zr vs. La/Sc diagram showing fields for tectonic settings (after Bhatia and Crook, 1986).

elements (i.e., Sm and Gd) are the common characteristics in shale samples. Taylor et al. (1983) found that sediments (shales, etc.) after the Archean are all negative Eu anomalies, while present-day high–temperature (> 250°C) geothermal systems, such as the rapidly expanding Pacific ridge, the slowly expanding Atlantic ridge, and the Laue Basin in the back-arc spreading center, are all positive Eu anomalies (Fouquet et al., 1993). Michard and Albarède (1986) also found that Eu can be reduced to a divalent state and thus fractionated with respect to other REEs at higher temperatures of > 200°C. Therefore, sediments formed under the influence of hydrothermal fluids may exhibit large positive Eu anomalies. This clear difference indicates that the studied samples are not related to the hydrothermal system. As discussed in Section 4.1, the depleted Eu is more likely controlled by the provenance rather than by hydrothermal events. Alexander et al. (2008) proposed that hydrothermal fluid possesses a chondritic Y/Ho value (~28) and higher Sm/Yb than modern seawater. The studied samples show relatively higher Sm/Yb than seawater and lower Y/Ho values close to hydrothermal fluid but the Eu/Sm ratios for the studied samples close to seawater and hydrogenesis Fe-Mn crusts (Fig. 9), all of which also indicate that the studied samples were affected but not controlled by hydrothermal fluid during their sedimentation processes.

Geologically, the large thickness of the Mesozoic–Cenozoic strata is unlikely to have hydrothermal fluids entering them (e.g., submarine hydrothermal fluid events), although there is a deep fracture developed in the study area (Fig. 1(a)). This is also illustrated by the immature maturity of the OM (Qiao et al., 2021). Another more important possibility is the input from hydrothermal fields. This possibility is very high because the spring water found in the northern Qaidam Basin indicates that

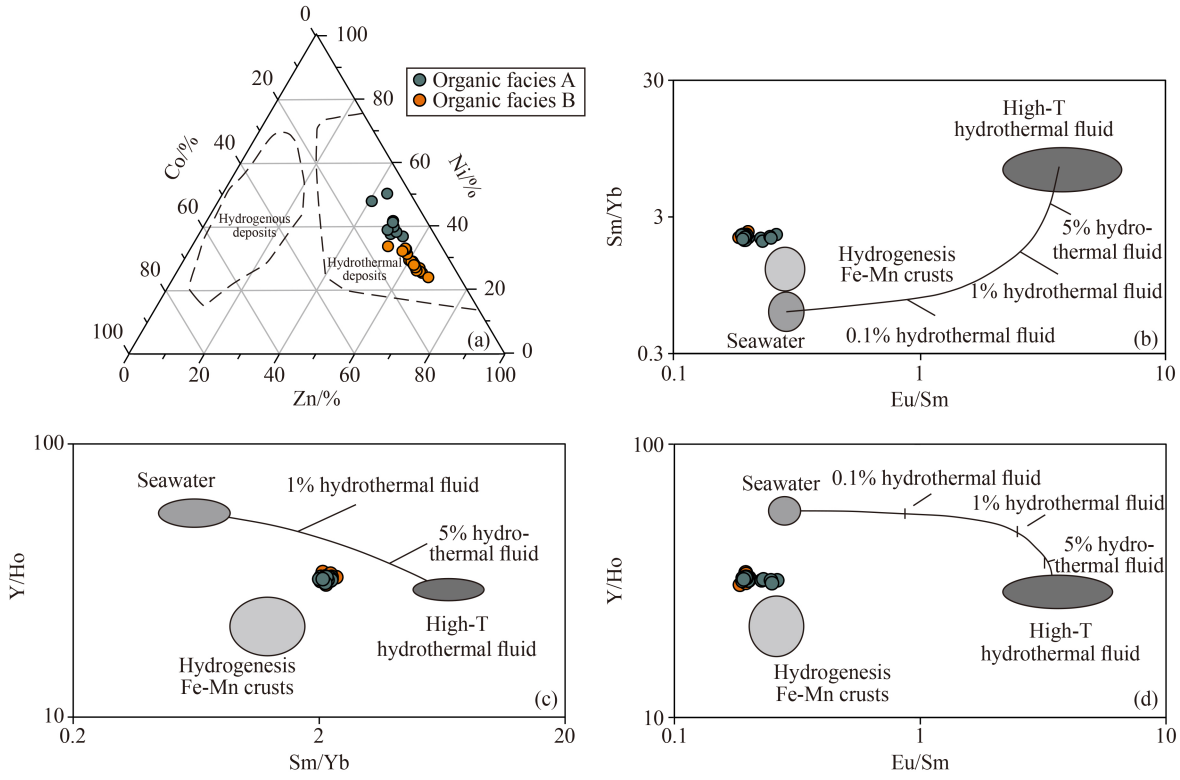

Fig. 9 (a) Ternary diagram of Co-Ni-Zn showing fields of hydrothermal and hydrogenous sediments (after Crerar, 1980), (b) Eu/Sm vs. Sm/Yb, (c) Sm/Yb vs. Y/Ho and (d) Eu/Sm vs. Y/Ho showing the effect of hydrogenous deposits/seawater interaction with variable degrees of hydrothermal fluids (b, c and d after Alexander et al., 2008).

this hydrothermal system is currently active (Stober et al., 2016). Stober et al. (2016) found that hot spring water is related to deep hydrothermal fluid-rock interactions, and is closely related to the tectonic activity (faulting) of the Qilian Mountains. Yu et al. (2013) found that the source of lithium in four salt lakes located in the Qaidam Basin is hydrothermal fields associated with a magmatic heat source, where two active faults converge in the upper reach of the Hongshui River. Much evidence indicates that the Qilian Mountains experienced significant orogenic growth and tectonic uplift after 11 Ma (e.g., Li et al., 2014; Meng et al., 2019; Zhuang et al., 2019), which may have enhanced the development of hydrothermal systems and led to the features of hydrothermal fluids in the studied samples. Therefore, the Ni–Zn–Co diagram reveals the hydrothermal origins came from hot springs developed with active faults around the basin.

In short, both organic facies A and B samples show some hydrothermal activity in the studied samples, which is more likely related to the hot spring water located at the margin of the basin rather than hydrothermal fluids from the deep faculty in the basin.

4.4 Palaeoredox conditions

Some trace elements, such as Th, V, Cr, Ni, and Co, are regarded as redox-sensitive elements and are thereby being widely used to evaluate palaeoredox situations (Jones and Manning, 1994; Tribovillard et al., 2006; Zhang et al., 2013; Qiao et al., 2020; Li et al., 2021a; Lv et al., 2021; Ali et al., 2022).

The ratios of U/Th and Ni/Co are sensitive for the studied samples, which show anoxic environments for organic facies A samples (U/Th ratio of 0.79–1.57 and Ni/Co ratio of 3.26–8.32) and oxic situations for organic facies B samples (U/Th ratio of 0.17–0.68 and Ni/Co ratio of 2.39–3.37) (Table 2). However, the proxies related to V including V/Cr and V/(V + Ni) show that both organic facies A and B samples are developed under oxic situations based on the threshold provided by previous studies (Table 2; Hatch and Leventhal, 1992; Jones and Manning, 1994), which are not suitable for the studied samples, especially for the organic facies A samples. The invalid results for the organic facies A samples might be due to low V concentrations compared to their high TOC contents. This might be due to the organism compositions for the studied samples. In general, V is easily absorbed and enriched by seawater planktonic algae (Shi et al., 2021) which only occupied a small proportion of the organic facies A samples (Qiao et al., 2021).

Due to the changeable valence state of Ce, Ce may oxidize in aqueous solution from the Ce^{3+} to the more insoluble Ce^{4+}, thus resulting in a positive Ce anomaly in sediments (German and Elderfield, 1990; Bellanca et al., 1997; Cullers, 2002; Wen et al., 2007; Li et al., 2021a).

Therefore, the value of Ce_{anom} was used to interpret the redox conditions when REEs were incorporated into the sediments (German and Elderfield, 1990). The Ce_{anom} value in modern seawater is 0.4–0.7 (Elderfield and Greaves, 1982), whereas the average Ce_{anom} value in mudstones is approximately 1.0 (Cox et al., 1995; Cullers and Berendsen, 1998). There are some methods to calculate Ce_{anom}. In this study, Ce_{anom} is defined as $Ce_n/(0.5 \times (La_n + Pr_n)$ (subscript n represents the PAAS-normalized value; the same for the following). In general, the Ce_{anom} values of < 0.5 indicates oxic, values between approximately 0.6–0.9 represent suboxic, and values > 0.9 indicate anoxic marine water (Chen et al., 2015).

The mudstones analyzed in this study show higher Ce_{anom} values of 0.96–1.00 with an average of 0.98 (Table 2; Fig. 10), indicating an anoxic environment for both organic facies A and B samples. For the organic facies A samples, the results based on Ce_{anom} values are consistent with the results based on relationships among TOC, TS and kinds of trace element concentrations (Qiao et al., 2021, 2022). In addition, the false appearance of Ce_{anom} values might be caused by La anomalies; therefore, the Ce_{anom} vs. Pr_{anom} ($Pr_n/(0.5 \times (Ce_n + Nd_n))$) plot is used to identify the reality of Ce_{anom} values (Nance and Taylor, 1976). The Ce_{anom} values of the studied samples indicate no obvious anomalies (Fig. 10(b)), indicating continuous anoxic conditions of the seawater (Pi et al., 2013). However, it is noteworthy that the redox conditions for organic facies B cannot be interpreted by Ce_{anom} values. Möller and Bau (1993) found that the stabilization of Ce (IV)–carbonate complexes can lead to positive Ce anomalies in the water column of alkaline lakes. This is a reasonable possibility for the positive Ce anomalies in organic facies B samples that developed in hypersaline environments (Qiao et al., 2021, 2022).

The Mn_{anmo} value is regarded as representative of redox conditions in sedimentary environments (Machhour et al., 1994; Bellanca et al., 1996; Cullers, 2002). The Mn_{anmo} value was calculated as $Mn_{anmo} = \log (Mn_n/Fe_n)$. Manganese is more likely to be accumulated in oxygenated conditions (Bellanca et al., 1996). Therefore, the less positive Mn_{anmo} values for the organic facies A samples ranging from −0.51–0.37 (−0.15 on average; Fig. 10) indicate that they were deposited in oxygen-depleted conditions, while the organic facies B samples have negative Mn_{anmo} values (−0.12–0.42 with an average value of 0.10), suggesting that they were deposited in oxygen-rich conditions. Although the studied samples derived from different environments do not show strong concentrations, as in previous studies (Qiao et al., 2021, 2022), the Mn_{anmo} can be regarded as a useful indicator of redox conditions.

4.5 Sedimentary rate

In fact, the rate of deposition is a key factor in controlling the production, degradation, and dilution of OM accumulation. Initially, OM accumulation increases with an increased sedimentation rate. When the sedimentation rate reaches a critical value, OM accumulation begins to

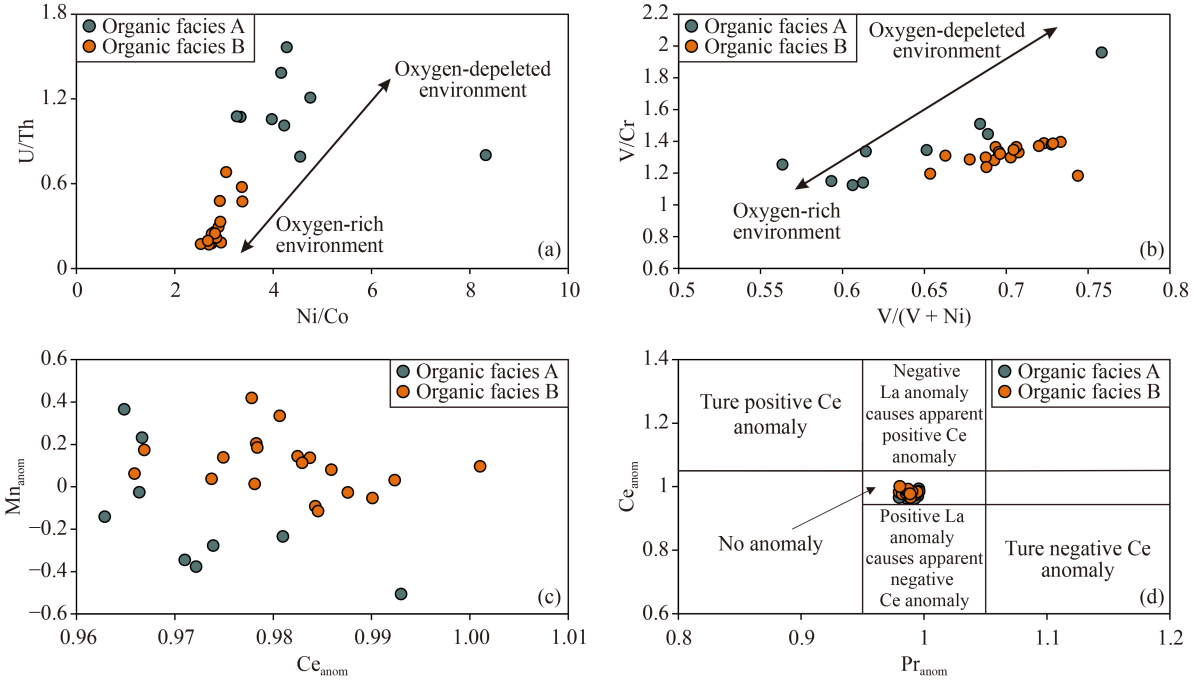

Fig. 10 Distribution of (a) U/Th vs. Ni/Co, (b) V/Cr vs. V/(V + Ni), (c) Ce_{anom} vs. Mn_{anom} and (d) Pr_{anom} vs. Ce_{anom} (after Bau and Dulski, 1996) in the studied samples, showing paleoredox conditions. $Mn_{anom} = \log (Mn_n/Fe_n)$; $Ce_{anom} = Ce_n/(0.5 \times (La_n + Pr_n))$, $Pr_{anom} = Pr_n/(0.5 \times (Ce_n + Nd_n))$.

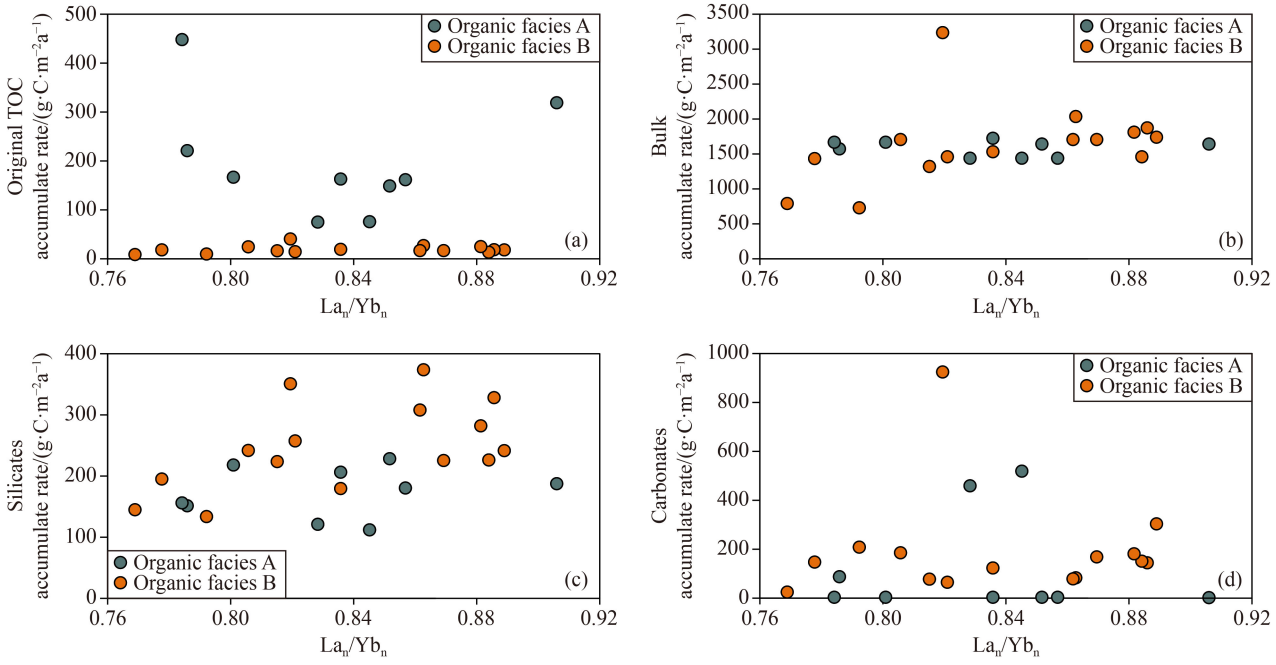

Fig. 11 La$_n$/Yb$_n$ vs. each accumulate rate of (a) original TOC, (b) bulk sample, (c) silicates and (d) carbonates for the studied samples. The accumulated rates are reported by Qiao et al., (2021).

decrease with the increase of the sedimentation rate. An excessively high sedimentation rate results in organic dilution, while an excessively low sedimentation rate leads to organic degradation in the oxidation process (Ibach, 1982; Stein, 1986; Tyson, 2001). Elemental geochemistry, especially for the REEs, can be used to analyze sedimentation rates (Elderfield and Greaves, 1982; Byrne and Kim, 1990; Zhang et al., 2013).

As the sedimentary environment changes, the electricity valence and adsorption capacity of REEs differ and can be perceived by the retention time during the deposition process. In general, LREEs are preferentially adsorbed by clay minerals and OM. Instead, HREEs form stable complexes in water columns (Byrne and Kim, 1990). It is believed that the differentiation degree of REEs is a response to the variation in sedimentation rates. When the particles are suspended in water columns for a short time, REEs are rapidly deposited with them, and there is less chance of exchange with seawater, showing weak differentiation. When suspended particles remain in lakes for a long time with low sedimentation rates, REEs decomposition in fine particles is promoted, and the REEs in the water column have enough time to be adsorbed by clay minerals and chemically react with OM, resulting in a significant differentiation of REEs (Elderfield and Greaves, 1982; Goldstein and Jacobsen, 1988; Johannesson et al., 1994). The La$_n$/Yb$_n$ values close to 1 (i.e., the La/Yb ratio in the studied samples close to that in the PAAS) indicate high sedimentation rates, while the low sedimentation rates are interpreted by deviating from 1 (Zhang et al., 2013). The La$_n$/Yb$_n$ values of 0.76–0.91 indicate high sedimentation rates, which is consistent with the average sedimentation rates of approximately 0.43 to 1.1 km/Ma. In addition, the average La$_n$/Yb$_n$ value for organic facies A samples (0.81) is smaller than that for organic facies B samples (0.84), which is consistent with the depositional conditions interpreted in previous studies (Qiao et al., 2021, 2022). However, it should be noted that the La and Yb concentrations are also affected by other issues (e.g., La/Yb, La/Th, La/Sc and Gd$_N$/Yb$_N$ used in this study and references there), so the La$_n$/Yb$_n$ value should be used with cautious. Actually, there are no clear differences in distribution range between organic facies A and organic facies B samples and no clear relationship between La$_n$/Yb$_n$ and accumulation rates (AR) of each bulk, original OM, silicates and carbonates reported by Qiao et al. (2021) (Fig. 11). These little disparities are consistent with little differences in the interpretation of provenance, palaeotectonic setting and hydrothermal activity based on two organic facies samples, which might indicate non–negligible provenance compositions.

5 Conclusions

This study focuses on trace elements and rare earth elements (REEs) geochemistry of the Pleistocene lacustrine mudstones in the central Qaidam Basin, and yields the following conclusions concerning the provenance area composition, palaeotectonic setting, hydrothermal activity, palaeoredox conditions and sedimentary rate.

1) The comparison shows that the two organic facies

samples developed different environments with completely different organic compositions and have strong geological interpretation consistency in the provenance of sediments, palaeotectonic setting, hydrothermal activity and sedimentary rate sedimentary rock.

2) The property of the provenance for the Pleistocene lacustrine mudstones was in the mixed area of sedimentary rock, granite and basalt, which is supported by the ΣREE vs. La/Yb discrimination diagram. In addition, sedimentary provenance from bivariate plots diagrams of Hf vs. La/Th and Th/Sc vs. Eu_{anom}, La/Co, Cr/Th, Gd_N/Yb_N and ΣLREE/ΣHREE show that the Pleistocene lacustrine mudstones were mainly derived from felsic sources.

3) Little contribution of ancient crustal sediments was supported by plot diagrams of Hf vs. La/Th and Zr/Sc vs. Th/Sc, and no ultramafic (ophiolitic) source was supported by plots of Cr vs. Ni and Cr/V vs. Y/Ni. Discriminant diagrams, consisting of La–Th–Sc and Th–Co–Zr/10, suggest that the mudstones of two organic facies were deposited in continental island arc tectonic settings, which is consistent with the tectonic evolution of the Cenozoic basin related to the India–Eurasia collision. A similar result can be drawn from the plot of Ti/Zr vs. La/Sc.

4) Both organic facies A and B samples show some hydrothermal origins based on the ternary diagram of Ni–Zn–Co and normalized REE patterns. This might indicate hydrothermal origins from hot springs related to active faults around the basin rather than the deep hydrothermal fluids entering the Qigequan Formation via deep faculties based on the comprehensive analyses of normalized REE patterns, negative Eu anomalies, Y/Ho, Sm/Yb and Eu/Sm.

5) Redox proxies including U/Th, Ni/Co and Mn_{anom} values indicate that most of the mudstones of the organic facies A samples were deposited under an oxygen-depleted condition, while the organic facies B samples were deposited under oxygen-rich conditions. In contrast, Ce_{anom} is unavailable for the organic facies B samples due to hypersaline environments, and V/Cr and V/(V + Ni) are invalid for the organic facies A samples, possibly because of their organism composition. The La_n/Yb_n values indicate high sedimentation rates, which is consistent with the average sedimentation rates of approximately 0.43 to 1.1 km/Ma. However, it should be noted that the La_n/Yb_n is also affected by the provenance of the studied samples.

Acknowledgments The study was granted financial support by the National Natural Science Foundation of China (Grant Nos. 42202154 and 42002050), and the Science Foundation of China University of Petroleum, Beijing (No. ZX20220074). Furthermore, we acknowledge four anonymous reviewers for the constructive comments on the original version of this manuscript.

References

Alexander B W, Bau M, Andersson P, Dulski P (2008). Continentally-derived solutes in shallow Archean seawater: rare earth element and Nd isotope evidence in iron formation from the 2.9 Ga Pongola Supergroup, South Africa. Geochim Cosmochim Acta, 72(2): 378–394

Ali F, Zhang S, Hanif M, Mohibullah M, Zhang Y, Usman M, Wang S, Liu X, Ma P, Huang D (2022). Geochemical investigation of low latitude black shale intervals of the Lower to Middle Jurassic succession, Indus Basin, Pakistan. Front Earth Sci, doi:10.1007/s11707-021-0943-4

Allègre C J, Minster J F (1978). Quantitative models of trace element behavior in magmatic processes. Earth Planet Sci Lett, 38(1): 1–25

An Z, Kutzbach J E, Prell W L, Porter S C (2001). Evolution of Asian monsoons and phased uplift of the Himalaya-Tibetan plateau since Late Miocene times. Nature, 411(6833): 62–66

Armstrong-Altrin J S, Verma S P (2005). Critical evaluation of six tectonic setting discrimination diagrams using geochemical data of Neogene sediments from known tectonic settings. Sediment Geol, 177(1–2): 115–129

Bao J, Wang Y, Song C, Feng Y, Hu C, Zhong S, Yang J (2017). Cenozoic sediment flux in the Qaidam Basin, northern Tibetan Plateau, and implications with regional tectonics and climate. Global Planet Change, 155: 56–69

Bau M, Dulski P (1996). Distribution of yttrium and rare-earth elements in the Penge and Kuruman iron-formations, Transvaal Supergroup, South Africa. Precambrian Res, 79(1–2): 37–55

Bellanca A, Claps M, Erba E, Masetti D, Neri R, Premoli Silva I, Venezia F (1996). Orbitally induced limestone/marlstone rhythms in the Albian—Cenomanian Cismon section (Venetian region, northern Italy): sedimentology, calcareous and siliceous plankton distribution, elemental and isotope geochemistry. Palaeogeogr Palaeoclimatol Palaeoecol, 126(3–4): 227–260

Bellanca A, Masetti D, Neri R (1997). Rare earth elements in limestone/marlstone couplets from the Albian-Cenomanian Cismon section (Venetian region, northern Italy): assessing REE sensitivity to environmental changes. Chem Geol, 141(3–4): 141–152

Bhat M I, Ghosh S K (2001). Geochemistry of the 2.51 Ga old Rampur group pelites, western Himalayas: implications for their provenance and weathering. Precambrian Res, 108(1–2): 1–16

Bhatia M R (1983). Plate tectonics and geochemical composition of sandstones. J Geol, 91(6): 611–627

Bhatia M R, Crook K A (1986). Trace element characteristics of graywackes and tectonic setting discrimination of sedimentary basins. Contrib Mineral Petrol, 92(2): 181–193

Byrne R H, Kim K H (1990). Rare earth element scavenging in seawater. Geochim Cosmochim Acta, 54(10): 2645–2656

Chen J, Algeo T J, Zhao L, Chen Z Q, Cao L, Zhang L, Li Y (2015). Diagenetic uptake of rare earth elements by bioapatite, with an example from Lower Triassic conodonts of south China. Earth Sci Rev, 149: 181–202

Choi J H, Hariya Y (1992). Geochemistry and depositional environment of Mn oxide deposits in the Tokoro Belt, northeastern Hokkaido. Japan. Econ Geol, 87(5): 1265–1274

Clark M K (2011). Early Tibetan Plateau uplift history eludes. Geology, 39(10): 991–992

Condie K C (1993). Chemical composition and evolution of the upper continental crust: contrasting results from surface samples and shales. Chem Geol, 104(1–4): 1–37

Cox R, Lowe D R, Cullers R L (1995). The influence of sediment recycling and basement composition on evolution of mudrock chemistry in the southwestern United States. Geochim Cosmochim Acta, 59(14): 2919–2940

Crerar D A (1980). Geochemistry of manganese: an overview. In: Varentsov I M, Grassely G, eds. Geology and Geochemistry of Manganese. Stuttgart: E'Schweizerbart'sche Verlag, Vol. l: 353–365

Cullers R L (1994). The controls on the major and trace element variation of shales, siltstones, and sandstones of Pennsylvanian-Permian age from uplifted continental blocks in Colorado to platform sediment in ansas, USA. Geochim Cosmochim Acta, 58(22): 4955–4972

Cullers R L (1995). The controls on the major- and trace-element evolution of shales, siltstones and sandstones of Ordovician to Tertiary age in the Wet Mountains Region, Colorado, USA. Chem Geol, 123(1–4): 107–131

Cullers R L (2000). The geochemistry of shales, siltstones, and sandstones of Pennsylvanian-Permian age, Colorado, USA: implications for provenance and metamorphic studies. Lithos, 51: 181–203

Cullers R L (2002). Implications of elemental concentrations for provenance, redox conditions, and metamorphic studies of shales and limestones near Pueblo, CO, USA. Chem Geol, 191(4): 305–327

Cullers R L, Barrett T, Carlson R, Robinson B (1987). Rare-earth element and mineralogic changes in Holocene soil and stream sediment: a case study in the Wet Mountains, Colorado, USA. Chem Geol, 63(3–4): 275–297

Cullers R L, Berendsen P (1998). The provenance and chemical variation of sandstones associated with the Mid-continent Rift System, USA. Eur J Mineral, 10(5): 987–1002

Cullers R L, Podkovyrov V N (2000). Geochemistry of the Mesoproterozoic Lakhanda shales in southeastern Yakutia, Russia: implications for mineralogical and provenance control, and recycling. Precambrian Res, 104(1–2): 77–93

Cullers R L, Podkovyrov V N (2002). The source and origin of terrigenous sedimentary rocks in the Mesoproterozoic Ui group, southeastern Russia. Precambrian Res, 117 (3–4): 157–183

Dang Y Q, Zhao W Z, Su A G, Zhang S C, Li M W, Guan Z Q, Ma D D, Chen X L, Shuai Y H, Wang H T, Tan Y H, Xu Z Y (2008). Biogenic gas systems in eastern Qaidam Basin. Mar Petrol Geol, 25: 344–356

Douville E, Bienvenu P, Charlou J L, Donval J P, Fouquet Y, Appriou P, Gamo T (1999). Yttrium and rare earth elements in fluids from various deep-sea hydrothermal systems. Geochim Cosmochim Acta, 63(5): 627–643

Douville E, Charlou J L, Oelkers E H, Bienvenu P, Jove Colon C F, Donval J P, Fouquet Y, Prieur D, Appriou P (2002). The rainbow vent fluids (36°14′N, MAR): the influence of ultramafic rocks and phase separation on trace metal content in Mid-Atlantic Ridge hydrothermal fluids. Chem Geol, 184(1–2): 37–48

Dupont-Nivet G, Krijgsman W, Langereis C G, Abels H A, Dai S, Fang X (2007). Tibetan plateau aridification linked to global cooling at the Eocene-Oligocene transition. Nature, 445(7128): 635–638

Elderfield H, Greaves M J (1982). The rare earth elements in seawater. Nature, 296(5854): 214–219

Fang X M, Zhang W L, Meng Q Q, Gao J J, Wang X M, King J, Song C H, Dai S, Miao Y F (2007). High-resolution magnetostratigraphy of the Neogene Huaitoutala section in the eastern Qaidam Basin on the NE Tibetan Plateau, Qinghai Province, China and its implication on tectonic uplift of the NE Tibetan Plateau. Earth Planet Sci Lett, 258(1–2): 293–306

Feng R, Kerrich R (1990). Geochemistry of fine-grained clastic sediments in the Archean Abitibi greenstone belt, Canada: implications for provenance and tectonic setting. Geochim Cosmochim Acta, 54(4): 1061–1081

Floyd P A, Leveridge B E, Franke W, Shail R, Dörr W (1990). Provenance and depositional environment of Rhenohercynian synorogenic greywackes from the Giessen Nappe, Germany. Geol Rundsch, 79(3): 611–626

Floyd P, Leveridge B (1987). Tectonic environment of the Devonian Gramscatho basin, south Cornwall: framework mode and geochemical evidence from turbiditic sandstones. J Geol Soc London, 144(4): 531–542

Fouquet Y, Charlou J L, von Stackelberg U, Wiedicke M, Erzinger J, Herzig P M, Muehe R (1993). Metallogenesis in back-arc environments: the Lau Basin example. Economic Geology, 88(8): 2154–2181

Garver J I, Royce P R, Smick T A (1996). Chromium and nickel in shale of the Taconic Foreland: a case study for the provenance of fine-grained sediments with an ultramafic source. J Sediment Res, 66: 100–106

Gehrels G, Kapp P, DeCelles P, Pullen A, Blakey R, Weislogel A, Ding L, Guynn J, Martin A, McQuarrie N, Yin A (2011). Detrital zircon geochronology of pre-Tertiary strata in the Tibetan–Himalayan orogen. Tectonics, 30(5): TC5016

German C R, Elderfield H (1990). Application of the Ce anomaly as a paleoredox indicator: the ground rules. Paleoceanography, 5(5): 823–833

Goldstein S J, Jacobsen S B (1988). Rare earth elements in river waters. Earth Planet Sci Lett, 89(1): 35–47

Hanson A D, Ritts B D, Zinniker D, Moldowan J M, Biffi U (2001). Upper Oligocene lacustrine source rocks and petroleum systems of the northern Qaidam basin, northwest China. AAPG Bull, 85: 601–619

Harrison T M, Copeland P, Kidd W S F, Yin A (1992). Raising tibet. Science, 255(5052): 1663–1670

Hatch J R, Leventhal J S (1992). Relationship between inferred redox potential of the depositional environment and geochemistry of the Upper Pennsylvanian (Missourian) Stark Shale Member of the Dennis Limestone, Wabaunsee County, Kansas, U. S. A. Chem Geol, 99(1–3): 65–82

Hiscott R N (1984). Ophiolitic source rocks for Taconic-age flysch:

trace element evidence. Geol Soc Am Bull, 95(11): 1261–1267

Hongo Y, Obata H, Gamo T, Nakaseama M, Ishibashi J, Konno U, Saegusa S, Ohkubo S, Tsunogai U (2007). Rare Earth Elements in the hydrothermal system at Okinawa Trough back-arc basin. Geochem J, 41(1): 1–15

Ibach L E J (1982). Relationship between sedimentation rate and total organic carboncontent in ancient marine sediments. AAPG Bull, 66: 170–188

Jian X, Guan P, Zhang W, Feng F (2013). Geochemistry of Mesozoic and Cenozoic sediments in the northern Qaidam Basin, northeastern Tibetan Plateau: implications for provenance and weathering. Chem Geol, 360-361: 74–88

Johannesson K H, Lyons W B, Bird D A (1994). Rare earth element concentrations and speciation in alkaline lakes from the western USA. Geophys Res Lett, 21(9): 773–776

Johnsson M J (1993). The system controlling the composition of clastic sediments. In: Johnsson M J, Basu A, eds. Processes Controlling the Composition of Clastic Sediments. Geological Society of America Special Paper, 284: 1–19

Jones B, Manning D A C (1994). Comparison of geochemical indices used for the interpretation of palaeoredox conditions in ancient mudstones. Chem Geol, 111(1–4): 111–129

Katz M E, Miller K G, Wright J D, Wade B S, Browning J V, Cramer B S, Rosenthal Y (2008). Stepwise transition from the Eocene greenhouse to the Oligocene icehouse. Nat Geosci, 1(5): 329–334

Kent-Corson M L, Ritts B D, Zhuang G, Bovet P M, Graham S A, Page Chamberlain C (2009). Stable isotopic constraints on the tectonic, topographic, and climatic evolution of the northern margin of the Tibetan Plateau. Earth Planet Sci Lett, 282(1–4): 158–166

Kutzbach J E, Prell W L, Ruddiman Wm F (1993). Sensitivity of Eurasian climate to surface uplift of the Tibetan Plateau. J Geol, 101(2): 177–190

LaMaskin T A, Dorsey R, Vervoort J D (2008). Tectonic controls on mudrock geochemistry, Mesozoic rocks of eastern Oregon and western Idaho, USA: implications for Cordilleran tectonics. J Sediment Res, 78(12): 765–783

Li J J, Fang X M, Song C H, Pan B T, Ma Y Z, Yan M D (2014). Late Miocene–Quaternary rapid stepwise uplift of the NE Tibetan Plateau and its effects onclimatic and environmental changes. Quat Res, 81(3): 400–423

Li J, Chen F, Ling Z, Li T (2021b). Lithium sources in oilfield waters from the Qaidam Basin, Tibetan Plateau: geochemical and Li isotopic evidence. Ore Geol Rev, 139: 104481

Li M, Fang X, Wang Z, Li J, Yan M, Galy A, Wang J, Lu S, Zhu L (2022). Using mineralogy and Sr-Nd isotopes of gypsum to constrain the provenance of sediments in the western Qaidam Basin, northern Tibetan Plateau: implications for neo-tectonic activities. J Asian Earth Sci, 223: 104983

Li Y, Wang Z, Wu P, Meng S (2021a). Paleoenvironment reconstruction of the upper paleozoic in the linxing area, northeastern Ordos Basin, China. AAPG Bull, 105(12): 2545–2574

Lv J, Zhang S, Yang N, Fu C, Yan X, Li Y (2021). Paleoenvironment controls on organic matter accumulation in transitional shales from the eastern Ordos Basin, China. Front Earth Sci, 15(4): 737–753

Möller P, Bau M (1993). Rare-earth patterns with positive cerium anomaly in alkaline waters from Lake Van, Turkey. Earth Planet Sci Lett, 117(3–4): 671–676

Machhour L, Philip J, Oudin J L (1994). Formation of laminite deposits in anaerobic—dysaerobic marine environments. Mar Geol, 117(1–4): 287–302

Mattinson C G, Wooden J L, Zhang J X, Bird D K (2009). Paragneiss zircon geochronology and trace element geochemistry, North Qaidam HP/UHP terrane, western China. J Asian Earth Sci, 35(3–4): 298–309

McCulloch M T, Wasserburg G J (1978). Sm-nd and rb-sr chronology of continental crust formation. Science, 200(4345): 1003–1011

McLennan S M (1989). Rare earth elements in sedimentary rocks: influence of provenance and sedimentary process. In: Lipin B R, McKay G A, eds. Geochemistry and Mineralogy of Rare Earth Elements. Rev Mineral, 21: 169–200

McLennan S M, Hemming S, McDaniel D K, Hanson G N (1993). Geochemical approaches to sedimentation, provenance, and tectonics. Special Papers-Geological Society of America: 21–40

McLennan S M, Taylor S R (1991). Sedimentary rocks and crustal evolution: tectonic setting and secular trends. J Geol, 99(1): 1–21

McLennan S M, Taylor S R, Eriksson K A (1983). Geochemistry of Archean shales from the Pilbara Supergroup, western Australia. Geochim Cosmochim Acta, 47(7): 1211–1222

McLennan S M, Taylor S R, McCulloch M T, Maynard J B (1990). Geochemical and Nd-Sr isotopic composition of deep-sea turbidites: crustal evolution and plate tectonic associations. Geochim Cosmochim Acta, 54(7): 2015–2050

Meng Q Q, Song C H, Nie J S, Liu C, He P J, Liu F B, Li L (2020). Middle-late Miocene rapid exhumation of the southern Qilian Shan and implications for propagation of the Tibetan Plateau. Tectonophysics, 77(5): 228279

Menold C A, Manning C E, Yin A, Tropper P, Chen X H, Wang X F (2009). Metamorphic evolution, mineral chemistry and thermobarometry of orthogneiss hosting ultrahighpressure eclogites in the North Qaidam metamorphic belt, western China. J Asian Earth Sci, 35(3–4): 273–284

Miao Y, Fang X, Herrmann M, Wu F, Zhang Y, Liu D (2011). Miocene pollen record of KC-1 core in the Qaidam Basin, NE Tibetan Plateau and implications for evolution of the East Asian monsoon. Palaeogeogr Palaeoclimatol Palaeoecol, 299(1–2): 30–38

Michard A, Albarède F (1986). The REE content of some hydrothermal fluids. Chem Geol, 55(1–2): 51–60

Molnar P, England P, Martinod J (1993). Mantle dynamics, uplift of the Tibetan plateau and the Indian monsoon. Rev Geophys, 31(4): 357–396

Nance W B, Taylor S R (1976). Rare earth element patterns and crustal evolution—I. Australian post-Archean sedimentary rocks. Geochim Cosmochim Acta, 40(12): 1539–1551

Nelson B K, DePaolo D J (1988). Comparison of isotopic and petrographic provenance indicators in sediments from Tertiary continental basins of New Mexico. J Sediment Res, 58(2): 348–357

Pang X, Zhao W, Su A, Zhang S, Li M, Dang Y, Xu F, Zhou R, Zhang D, Xu Z, Guan Z, Chen J, Li S (2005). Geochemistry and origin of the giant Quaternary shallow gas accumulations in the eastern Qaidam Basin, NW China. Org Geochem, 36(12): 1636–1649

Pi D H, Liu C Q, Shields-Zhou G A, Jiang S Y (2013). Trace and rare earth element geochemistry of black shale and kerogen in the early Cambrian Niutitang Formation in Guizhou Province, south China: constraints for redox environments and origin of metal enrichments. Precambrian Res, 225: 218–229

Piepgras D J, Jacobsen S B (1992). The behavior of rare earth elements in seawater: precise determination of variations in the North Pacific water column. Geochim Cosmochim Acta, 56(5): 1851–1862

Qiao J, Grohmann S, Baniasad A, Zhang C, Jiang Z, Littke R (2021). High microbial gas potential of Pleistocene lacustrine deposits in the central Qaidam Basin, China: an organic geochemical and petrographic assessment. Int J Coal Geol, 245: 103818

Qiao J, Littke R, Grohmann S, Zhang C, Jiang Z, Strauss H, Zieger L (2022). Climatic and environmental conditions during the Pleistocene in the Central Qaidam Basin, NE Tibetan Plateau: evidence from GDGTs, stable isotopes and major and trace elements of the Qigequan Formation. Int J Coal Geol, 254: 103958

Qiao J, Liu L, Shang X (2020). Deposition conditions of the jurassic lacustrine source rocks in the East Fukang sag, Junggar Basin, NW China: evidence from major and trace elements. Geol J, 55(7): 4936–4953

Qiu N, Kang Y, Jin Z (2003). Temperature and pressure field in the Tertiary succession of the western Qaidam Basin, northeast Qinghai-Tibet Plateau, China. Mar Pet Geol, 20(5): 493–507

Ramstein G, Fluteau F, Besse J, Joussaume S (1997). Effect on orogeny, plate motion and land–sea distribution on Eurasian climate change over the past 30 million years. Nature, 386(6627): 788–795

Rieser A B, Liu Y, Genser J, Neubauer F, Handler R, Friedl G, Ge X H (2006a). $^{40}Ar/^{39}Ar$ ages of detrital white mica constrain the Cenozoic development of the intracontinental Qaidam Basin, China. Geol Soc Am Bull, 118(11–12): 1522–1534

Rieser A B, Liu Y, Genser J, Neubauer F, Handler R, Ge X H (2006b). Uniform Permian $^{40}Ar/^{39}Ar$ detrital mica ages in the eastern Qaidam Basin (NW China): where is the source? Terra Nova, 18(1): 79–87

Rieser A B, Neubauer F, Liu Y, Ge X (2005). Sandstone provenance of north-western sectors of the intracontinental Cenozoic Qaidam basin, western China: tectonic vs. climatic control. Sediment Geol, 177(1–2): 1–18

Ritts B D, Biffi U (2001). Mesozoic northeast Qaidam basin: response to contractional reactivation of the Qilian Shan, and implications for the extent of Mesozoic intracontinental deformation in central Asia. Mem Geol Soc Am, 194: 293–316

Roser B P, Korsch R J (1986). Determination of tectonic setting of sandstone-mudstone suites using SiO_2 content and K_2O/Na_2O ratio. J Geol, 94(5): 635–650

Royden L H, Burchfiel B C, van der Hilst R D (2008). The geological evolution of the Tibetan Plateau. Science, 321(5892): 1054–1058

Ryan K M, Williams D M (2007). Testing the reliability of discrimination diagrams for determining the tectonic depositional environment of ancient sedimentary basins. Chem Geol, 242(1–2): 103–125

Shi C, Cao J, Han S, Hu K, Bian L, Yao S (2021). A review of polymetallic mineralization in lower Cambrian black shales in South China: combined effects of seawater, hydrothermal fluids, and biological activity. Palaeogeogr Palaeoclimatol Palaeoecol, 561: 110073

Shi C, Yan M, Chi Q (2007). Abundances of chemical elements of the granitoids in different geotectonic units of China and their characteristics. Front Earth Sci China, 1(3): 309–321

Shuai Y, Zhang S, Grasby S E, Chen Z, Ma D, Wang L, Li Z, Wei C (2013). Controls on biogenic gas formation in the Qaidam Basin, northwestern China. Chem Geol, 335: 36–47

Song S G, Zhang L F, Niu Y L, Su L, Jian P, Liu D Y (2005). Geochronology of diamondbearing zircons from garnet peridotite in the North Qaidam UHPM belt, Northern Tibetan Plateau: a record of complex histories from oceanic lithosphere subduction to continental collision. Earth Planet Sci Lett, 234(1–2): 99–118

Song S, Su L, Niu Y, Zhang G, Zhang L (2009). Two types of peridotite in North Qaidam UHPM belt and their tectonic implications for oceanic and continental subduction: a review. J Asian Earth Sci, 35(3–4): 285–297

Stein R (1986). Organic carbon and sedimentation rate–further evidence for anoxic deep-water conditions in the Cenomanian/ Turonian Atlantic Ocean. Mar Geol, 72(3–4): 199–209

Stober I, Zhong J, Zhang L, Bucher K (2016). Deep hydrothermal fluid-rock interaction: the thermal springs of Da Qaidam, China. Geofluids, 16(4): 711–728

Sun J, Ye J, Wu W, Ni X, Bi S, Zhang Z, Liu W, Meng J (2010). Late Oligocene-Miocene mid-latitude aridification and wind patterns in the Asian interior. Geology, 38(6): 515–518

Sun Q, Wang Z, Chen J, Feng W (2009). Climate implications of major geochemical elements in the Holocene sediments of the North and East China monsoonal regions. Front Earth Sci, 3(3): 291–296

Tapponnier P, Zhiqin X, Roger F, Meyer B, Arnaud N, Wittlinger G, Jingsui Y (2001). Oblique stepwise rise and growth of the Tibet Plateau. Science, 294(5547): 1671–1677

Taylor S R, McLennan S M (1985). The Continental Crust: Its Composition and Evolution. London: Blackwell Scientific

Taylor S R, McLennan S M, McCulloch M T (1983). Geochemistry of loess, continental crustal composition and crustal model ages. Geochim Cosmochim Acta, 47(11): 1897–1905

Tribovillard N P, Algeo T J, Lyons T, Riboulleau A (2006). Trace metals as paleoredox and paleoproductivity proxies: an update. Chem Geol, 232(1–2): 12–32

Tyson R V (2001). Sedimentation rate, dilution, preservation and total organic carbon: some results of a modelling study. Org Geochem, 32(2): 333–339

Wang C, Zhao X, Liu Z, Lippert P C, Graham S A, Coe R S, Yi H, Zhu L, Liu S, Li Y (2008). Constraints on the early uplift history of the Tibetan Plateau. Proc Natl Acad Sci USA, 105(13): 4987–4992

Wang T, Yang S, Duan S, Chen H, Liu H, Cao J (2015). Multi-stage primary and secondary hydrocarbon migration and accumulation in lacustrine jurassic petroleum systems in the northern Qaidam Basin, NW China. Mar Pet Geol, 62: 90–101

Wen H, Zheng R, Geng W, Fan M, Wang M (2007). Characteristics of rare earth elements of lacustrine exhalative rock in the Xiagou Formation of Lower Cretaceous in Qingxi sag, Jiuxi Basin. Front Earth Sci China, 1(3): 333–340

Wu Z, He S, He Z, Li X, Zhai G, Huang Z (2022). Petrographical and

geochemical characterization of the Upper Permian Longtan formation and Dalong Formation in the Lower Yangtze region, South China: implications for provenance, paleoclimate, paleoenvironment and organic matter accumulation mechanisms. Mar Pet Geol, 139: 105580

Yin A, Harrison T M (2000). Geologic evolution of the Himalayan–Tibetan orogen. Annu Rev Earth Planet Sci, 28(1): 211–280

Yu J, Gao C, Cheng A, Liu Y, Zhang L, He X (2013). Geomorphic, hydroclimatic and hydrothermal controls on the formation of lithium brine deposits in the Qaidam Basin, northern Tibetan Plateau, China. Ore Geol Rev, 50: 171–183

Zhang G, Song S, Zhang L, Niu Y (2008). The subducted oceanic crust within continental-type UHP metamorphic belt in the north Qaidam, NW China: evidence from petrology, geochemistry and geochronology. Lithos, 104(1–4): 99–118

Zhang J X, Mattinson C G, Meng F C, Yang H J, Wan Y S (2009). U–Pb geochronology of paragneisses and metabasite in the Xitieshan area, north Qaidam Mountains, western China: constraints on the exhumation of HP/UHP metamorphic rocks. J Asian Earth Sci, 35(3–4): 245–258

Zhang M, Liu Z, Xu S, Sun P, Hu X (2013). Element response to the ancient lake information and its evolution history of argillaceous source rocks in the Lucaogou Formation in Sangonghe Area of Southern Margin of Junggar Basin. J Earth Sci, 24(6): 987–996

Zhang S C, Li M W, Shuai Y H, Huang L, Su A G, Li Z X (2014). Biogeochemical identification of the Quaternary biogenic gas source rock in the Sanhu Depression, Qaidam Basin. Org Geochem, 73: 101–108

Zhang S C, Shuai Y H, Huang L, Wang L Q, Su J, Huang H P, Ma D D, Li M W (2013a). Timing of biogenic gas formation in the eastern Qaidam Basin, NW China. Chem Geol, 352: 70–80

Zhuang G, Hourigan J K, Koch P L, Ritts B D, Kent-Corson M L (2011a). Isotopic constraints on intensified aridity in Central Asia around 12 Ma. Earth Planet Sci Lett, 312(1–2): 152–163

Zhuang G, Hourigan J K, Ritts B D, Kent-Corson M L (2011b). Cenozoic multiple-phase tectonic evolution of the northern Tibetan Plateau: constraints from sedimentary records from Qaidam Basin, Hexi Corridor, and Subei Basin, northwest China. Am J Sci, 311(2): 116–152

Zhuang G, Zhang Y G, Hourigan J, Hourigan J, Ritts B, Hren M, Hou M, Wu M, Kim B (2019). Microbial and geochronologic constraints on the Neogene paleotopography of northern Tibetan Plateau. Geophys Res Lett, 46(3): 1312–1319